THESIS

A MICROPHYSIOLOGICAL SYSTEM FOR STUDYING BARRIER HEALTH OF LIVE TISSUES IN REAL TIME

Submitted by

Ryan Way

Department of Electrical and Computer Engineering

In partial fulfillment of the requirements

For the Degree of Master of Science

Colorado State University

Fort Collins, Colorado

Spring 2024

Master's Committee:

Advisor: Thomas W. Chen

Jesse Wilson
Adam Chicco

ABSTRACT

A MICROPHYSIOLOGICAL SYSTEM FOR STUDYING BARRIER HEALTH OF LIVE TISSUES IN REAL TIME

Epithelial cells create barriers that protect many different components in the body from their external environment. The gut in particular carries bacteria and other infectious agents. A healthy gut epithelial barrier prevents unwanted substances from accessing the underlying lamina propria while maintaining the ability to digest and absorb nutrients. Increased gut barrier permeability, better known as leaky gut, has been linked to several chronic inflammatory diseases. Yet understanding the cause of leaky gut and developing effective interventions are still elusive due to the lack of tools to maintain tissue's physiological environment while elucidating cellular functions under various stimuli ex vivo. This thesis presents a microphysiological system capable of recording real-time barrier permeability of mouse gut tissues in a realistic physiological environment over extended durations. Key components of the microphysiological system include a microfluidic chamber designed to hold the live tissue explant and create a sufficient microphysiological environment to maintain tissue viability; proper media composition that preserves a microbiome and creates necessary oxygen gradients across the barrier; integrated sensor electrodes and supporting electronics for acquiring and calculating transepithelial electrical resistance (TEER); and a scalable system architecture to allow multiple chambers running in parallel for increased throughput. The experimental results demonstrate that the system can maintain tissue viability for up to 72 hours. The results also show that the custom-built and integrated TEER sensors are sufficiently sensitive to distinguish differing levels of barrier permeability when treated with collagenase and low pH media compared to control. Permeability variations in tissue explants from different positions in the intestinal tract were also investigated using TEER revealing their disparities in permeability. Finally, the results also quantitatively determine the effect of the muscle layer on total epithelial resistance.

ACKNOWLEDGEMENTS

First and foremost, I would like to thank my professor Dr. Chen and my colleague Ming-Hao Cheng for their help and guidance at every stage in the design process. I would also like to thank Dr. Tobet, Hayley Templeton, Amanda Cherwin, Alexis Ehrlich, and Connie King for their contributions in all live tissue biological experiments. They performed all the tissue preparation/sectioning/imagery, dissection, media preparation, and much more. They also provided useful discussions on microfluidic device design.

TABLE OF CONTENTS

LIST OF TABLES

LIST OF FIGURES

Chapter 1 – Introduction

Epithelial cells are the body's first line of defense for protecting the host from its ex-ternal environment. The reliability of these barriers is extremely important in the body's continued health and homeostasis. This makes the continued health and drug response of epithelial layers, specifically in the gut, an important field of study for researchers. There are many different types of barriers in the body, the most important include skin, intestinal, and the blood brain barrier (BBB). Many devices and methods have been created and investigated to study the epithelial layers as they would be in the body. The main goal of these devices being to replicate the environment and organ in vivo to then study the cellular transport processes for drug discovery and many other reasons. The current devices made for epithelial/endothelial barrier research come in three different categories. The first device is what's called an "Ussing Chamber"[1]–[7], this device is made to hold a live tissue explant of epithelial cells, this device creates an ex vivo environment. The second category is where the epithelial (or endothelial) cells are cultured on a semi-permeable membrane inside of a well-plate dish, this means the barrier cells are studied in an in vitro environment [8]–[14]. This type of experiment is done mostly in the Transwell® system. The third and final category is called Organ-on-a-chip (OoC) system [9], [10], [15]–[21]. The OoC device is a more advanced system which incorporates microfluidics for maintaining the physiological condition within the system. Microfluidics create such a physiological condition around cells to maintain their viability during a required period for study.

To quantify the integrity of tight junctions of an epithelial barrier, many researchers have performed experiments to find the transepithelial/transendothelial electrical resistance (TEER). TEER values are widely accepted measures of the integrity of cellular barriers that are non-invasive and able to monitor live cells throughout an experiment. TEER values are often supported using fluorescently labelled probes to visualize the paracellular flux across the epithelium. Ussing chambers, Transwell®, and OoC devices are very often modified to have electrodes that can record TEER across the barrier being investigated. Most of the prior research using TEER has been on the in vitro models (Transwell® and OoC) of epithelium. This is an attractive method because of the high throughput and the freedom of growing the cell monolayer in a controlled environment. The downside to using in vitro cell monolayers is that they are unable to represent the full cellular complexity of the organs in vivo.

Live tissue in an ex vivo environment provides a much more accurate physiological model. Ex vivo epithelial/endothelial models can include the full variety of cells through-out the barrier, this is something that can't

be replicated in cell culture experiments. However, working with ex vivo tissue also comes several difficulties. These difficulties include tissue dissection/preparation, tissue viability, sterilization, and added diffusion layer resistance. With reduced ability to maintain tissue's viability, experiments on live tissue in an Ussing chamber have often been limited to under 5 hours [2], [11]. To develop more physiologically relevant ex vivo models it is important to improve tissue viability. This allows experiments to be conducted after the tissue has settled into its new environment inside the chamber. This can be achieved through the addition of microfluidics and appropriate media composition in the ex vivo device. Microfluidics create a more accurate physical environment for the live tissue explant and the media composition provides the tissue with appropriate nutrients appropriately mimicking its in-vivo counterparts.

Current devices that incorporate microfluidics with ex vivo tissue have been able to overcome many of the difficulties that previously hindered ex vivo experiments. This includes longer tissue viability, more physiologically accurate microenvironments, and improved ex vivo models [22]. However, the design considerations needed for these devices are often challenging and specific to the goal of the research. Some of these include micro-dissected tissue samples to load tissues into primed microfluidic channels [23], using subatomic pressure to conform outer surfaces to perfusion channels [24], using petroleum jelly or quick setting epoxy to form a seal around a tissue to create a dual flow barrier [25]–[27], and suturing intestinal tissue to a fluidic port [28]. The devices that are designed to model barrier functions [22], [24]–[28], generally require special considerations to create the isolated dual flow making them have low-throughput. Another issue with these current devices is the lack of real-time measurements, with no integrated sensors for electrical measurement. To examine the health of the tissue, the experiment is broken down and the tissue must undergo lengthy post-processing. These downfalls create avenues for newer and more advanced devices to keep improving ex vivo models in the field of biomedical engineering.

The research in this thesis presents a scalable microfluidic platform for ex vivo tissue with microfluidics, integrated sensors, and electronics. We show experimental results that demonstrate the system's ability to maintain tissue viability for up to 72 hours. We also show that the custom-designed TEER sensors and the supporting electronics are sufficiently sensitive to distinguish differing levels of barrier permeability when treated with collagenase and low pH media compared to control, as well as permeability variations in tissue explants from different positions in the intestinal tract. Our contribution is threefold: first, the microfluidics are designed to take into account flow patterns and shear stress that mimic the in vivo environment and help keep the tissue explants viable much longer than what

has been achieved so far; second, the TEER measurement of the tissue explants is supported by integrated electrodes and the custom-designed and portable backend electronics to record real-time TEER measurements throughout the entirety of the experiment at a user-specified interval, thus, allowing researchers to observe the evolution of the barrier integrity without stopping the experiment; third, the system architecture is fully scalable allowing multiple Ussing chambers to be connected to the integrated system in a plug-and-play fashion to increase throughput, while maintaining its portability. All these features are important to further advance biomedical research and drug discovery.

Chapter 2 – Background and Current Technology

2.1. Epithelial Tissue

Epithelial cells are throughout the body performing several important jobs. They are what lines all surfaces inside your body and form a type of barrier. Mainly, the epithelial cells are there to provide the first line of defense for protecting the mammalian host from its external environment [29]. Other functions include secretion, absorption, filtration, diffusion, and more. The most important epithelial barriers include the skin, gastrointestinal, and respiratory tracts. It is very important for the mammalian hosts' health and homeostasis that these epithelial barriers are healthy. Therefore, this area has attracted a lot of attention for disease modelling and drug discovery. The focus of the research presented in this thesis was specifically on studying the intestinal epithelium health of mice.

The epithelial sheets are formed by cells that are attached to each other, thus providing a physical barrier. However, these surfaces are very complex, and include many chemical and biological obstacles.

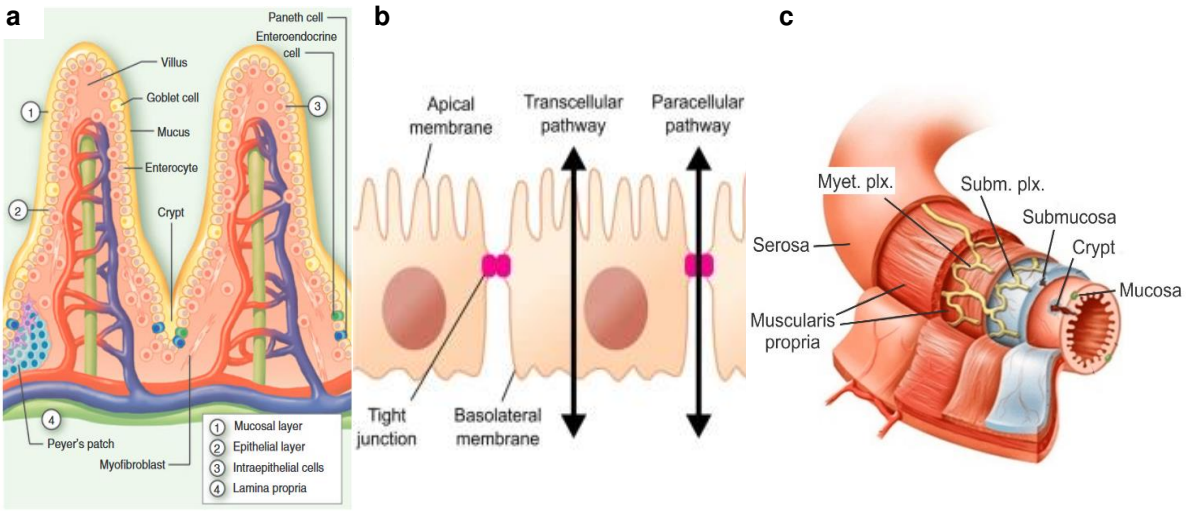

Figure 2.1: **a)** Structural Organization of intestinal mucosal barrier [29]; b) Paracellular and transcellular pathways across an epithelial layer [14]; **c)** Layered Structure of the large intestine [30]

Figure 2.1a shows a cross section view of the intestinal mucosal barrier, inside of this barrier is the epithelial layer. It shows the vast biological complexity of not only the epithelial layer, but also the surrounding cells and tissue. **Figure 2.1b** is a close-up view of the epithelial layer. There are two sides to the epithelial layer, the apical membrane, and the basolateral membrane. The apical membrane is the "outside", facing the lumen. For the intestine, this means that the apical membrane is on the inside of the gastrointestinal tract. The basolateral membrane faces the "inside" of the

mucosal barrier and the neighboring cells. **Figure 2.1c** shows all the layers of the large intestine structure outside of the mucosal barrier. These extra diffusion layers include the submucosa, muscle layers, and the serosa. These added layers of protection for the gastrointestinal tract are very important to the health of the host, so they need to be considered by any researcher studying the intestinal barrier. It is generally accepted that the tighter the epithelial cells are packed in the epithelial layer (i.e., the permeability), the healthier the intestine is. The TEER measurement (detailed later in this chapter) can discover changes in the epithelial layer that are caused by diseases and effects of therapeutics on the epithelial layer.

2.2. Ussing Chamber

The Ussing Chamber, named after the Danish biologist Hans Ussing, was invented in the 1950's [1]. This device was originally designed to understand the phenomenon of active NaCl transport across frog skin. Ussing and his colleagues dissected frog skin and mounted it between two separate chambers that hold identical electrolyte solutions. By doing this they were able to distinguish the movement of ions done by the epithelial cells from the ion transport through paracellular pathways. This technique set the groundwork and created the first model of epithelial transport. More modern designs of Ussing systems have been made to accommodate many different types of epithelial barriers inside an animal. These barriers include skin, intestinal, esophageal, and more [2], [4], [6], [31]. The Ussing chamber device is the most used tool for ex-vivo measurements of epithelial permeability, through paracellular flux or electrical measurements. **Figure 2.2** shows three different Ussing chamber designs. **Figure 2.2a** is the original Ussing chamber design created by Hans Ussing. In this original design, the piece of frog skin was secured between two reservoirs. By doing this, each reservoir half is completely isolated from the other allowing for the transport processes to be studied. Using a battery and potentiometer, the voltage across the tissue is held at zero volts. Then the resulting short-circuit current is read through a microammeter. The voltage clamp and current readings are done through Agar-Ringer salt bridges connected to the reservoir baths. **Figure 2.2b** is another classic Ussing chamber design for mouse intestinal tissue. This design was intended to replicate and improve the original design by Ussing et al. This design is an improvement because of the gas lift circulation, heated water jacket, and the ability to hold live mouse intestinal slices. While this design is an improvement of the original Ussing chamber, there are still disadvantages that remain. These include bulkiness, low throughput, external benchtop equipment, and complex setup. Finally, **Figure 2.2c** is a more modern Ussing chamber design. This design uses Ag/AgCl chopstick electrodes and smaller reservoir baths to reduce the size and increase throughput of the device. This device also includes its own electrical manifold to perform

electrical measurements on the Ussing chambers. The reservoir baths can be circulated, which increases the viability of the tissue slightly [22], but creates an uncontrollable microenvironment.

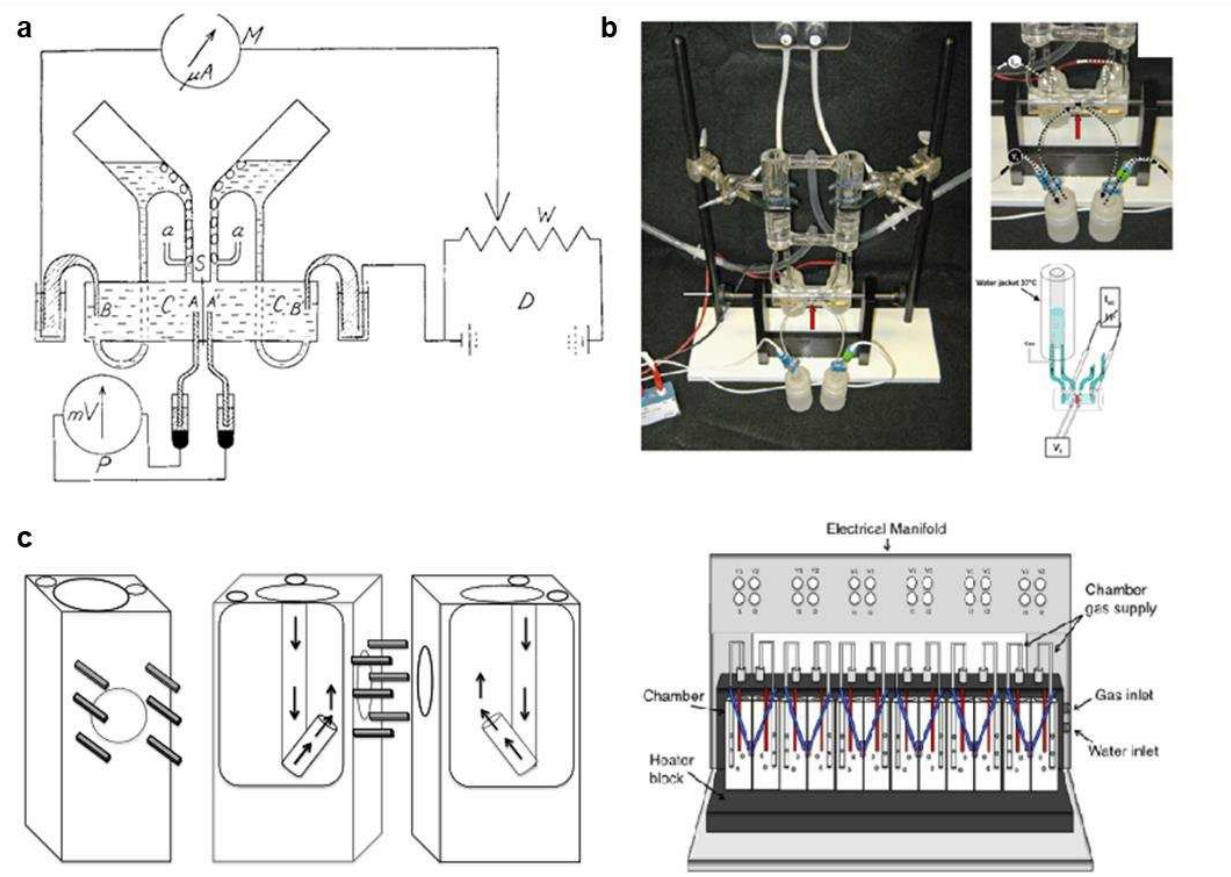

Figure 2.2: a) Original (1950) Ussing Chamber Design by Hans Ussing [1]; **b)** Classic (2009) example of an Ussing chamber design [2]; **c)** Modern (2019) example of an Ussing chamber [6]

Ussing chamber studies of the intestine epithelia is a common choice for researchers because of its importance and links to known health issues inside the body. It was intestinal Ussing chamber studies that helped reveal the mechanistic processes of cystic fibrosis. Using the Ussing chamber they showed that Cl^- secretion was decreased in patients due to a mutated CFTR gene [5], [6], [32]–[34]. While the Ussing chamber has made many great discoveries about the epithelial transport process, it is easy to tell that the design has not evolved much since the 1950's. There are several key disadvantages to the Ussing Chamber. These disadvantages include complexity of tissue sample preparation, requiring expensive benchtop measurement equipment; having static media in the chamber resulting in low tissue viability; being low throughput; having a bulky setup. These issues have turned

many researchers away from using the Ussing chamber and towards a device that is designed for an in vitro epithelial cell monolayer. These in vitro devices will be discussed in the next section.

2.3. In Vitro Epithelial Layer Models

2.3.1. Transwell System

An alternative method to study the epithelial cells transport process and permeability without using live tissues (ex vivo) is by using cultured in vitro epithelial cell monolayers. The most common and simple method to create in vitro barrier is by using a transwell insert [8]–[14] as shown in **Figure 2.3**. The transwell insert is designed to be placed inside of a typical well plate. It works by having a porous membrane at the bottom of the well where cell cultures can grow creating the epithelial barrier. The porous membrane creates a path for particles to diffuse through the membrane pores. Another important aspect of the transwell systems is that the epithelial cell culture has a basal and apical compartment. This allows the cells to uptake and secret molecules, which is very important in creating an environment that better mimics in vivo barriers [14]. The barrier characteristics of the epithelial monolayer can be measured in terms of TEER using the chopstick electrodes as shown in Figure 3.

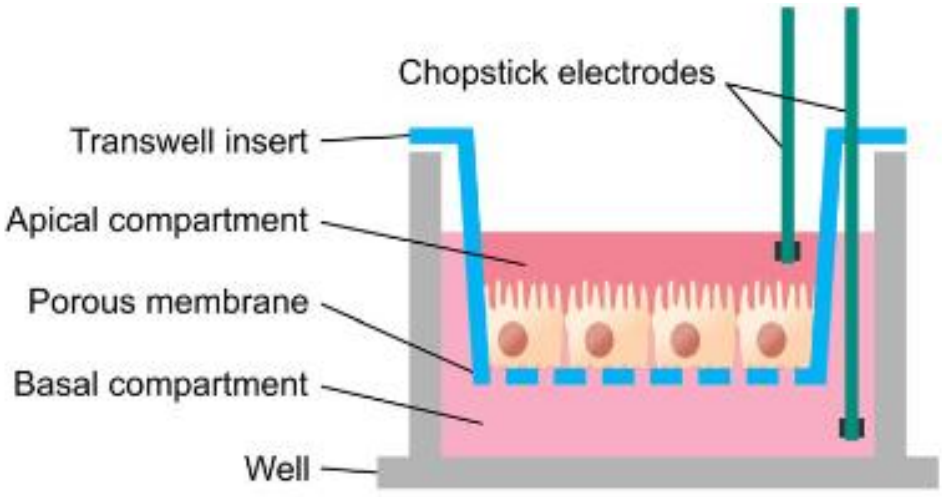

Figure 2.3: Transwell Insert System [14]

Transwell systems are widely used to study barrier functions because of their commercial availability and their ease of use, however they are limited to studying monolayers, not live tissues. The physiology between monolayers and live tissues is very different. Another important limitation with the transwell is that there is no media flow on either side of the barrier. This limits the viability of the cells and isn't accurate to how the physiological environment would

be in vivo. The device that addresses this issue is discussed in Section 2.3.2. Furthermore, the electrical measurements in a Transwell system using Chopstick electrodes are not the ideal method because they make it hard to reproduce measurements. This is because distance from the cell monolayer is very important and chopstick electrodes are hard to place in the exact same position for every experiment. The electrical measurement that is being taken place will be discussed later in Section 2.5.

2.3.2. Organ-on-a-chip Devices

An Organ-on-a-chip (OoC) device is a more modern solution to the transwell insert. A miniature tissue is typically grown on a microfluidic chip inside an OcO device. This in vitro cell culture can better mimic human physiology than the transwell both biochemically and physically [15]. The creation of microfluidic channels to form a microenvironment for the cell culture to grow allows for this device to better replicate in vivo environments. An example of this is that the cell cultures in a OoC undergo shear stress from the fluid flow set by the researcher. This is a physical attribute that is also present in vivo. Another benefit is that OoC devices allow for electrodes to be integrated. This is a preferable alternative to the chopstick electrodes in the transwell because the measurements become much more repeatable [21]. An example of an OoC device can be seen in **Figure 2.4**.

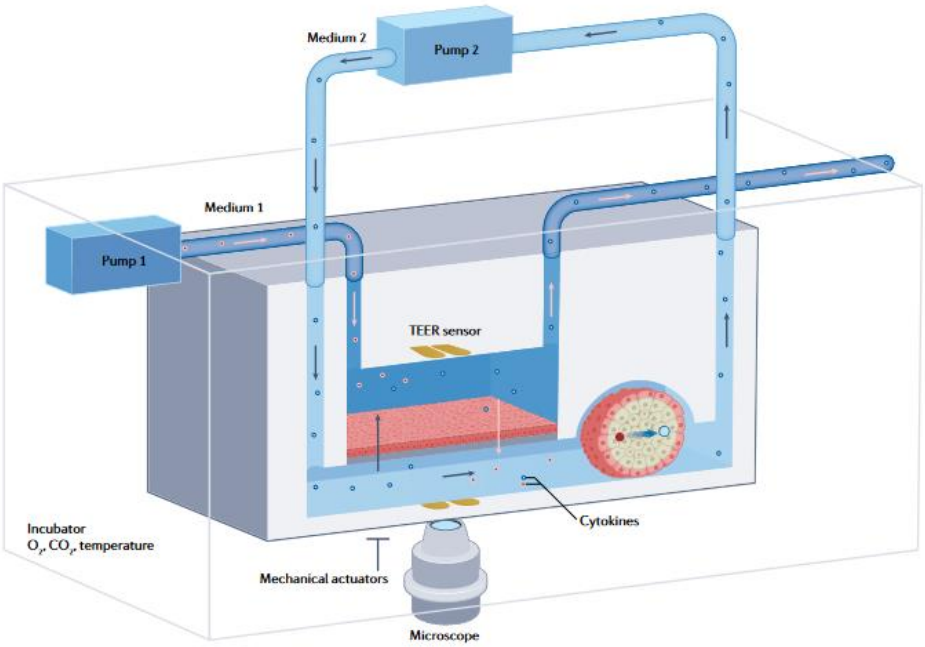

Figure 2.4: Organ-on-a-chip Device example [15]

The microfluidics and the associated microenvironment of OoC devices make it a more physiologically relevant model. Even though miniature tissues are grown in OoC devices, they are still not at the complexity of live tissues, and therefore, not representative of biological functions live tissues can demonstrate. Furthermore, growing miniature tissues in OoC devices increase the complexity and difficulty of designing and performing experiments [9], [16], [17], [19], [20].

2.3.3. In Vitro vs. Ex Vivo Experiments

In simple terms the difference between in vitro and ex vivo experiments is that ex vivo experiments use live tissue explants taken from an animal and in vitro experiments are cell cultures grown in the lab. Both types of experiments are trying to replicate the physiology in vivo of an organ or epithelial barrier in question. Over the years of transport process research, most researchers have decided to work with in vitro cell monolayers because they are easier to work with and they have a higher throughput due to the availability of commercial platforms. The main disadvantage of working with in vitro cells is that they are unable to replicate the full complexity of the organ and its environment in vivo. This limits the translatability of the results from these experiments to answering key questions about the target organ in vivo. Ex vivo tissues in general provide a more realistic platform allowing experiments to be performed in a more physiologically realistic model. For studying epithelial barrier, ex vivo tissues include all the different cell types as they would be in vivo, and it also includes the extra layers of diffusion that can't be grown in an in vitro experiment. This includes the extra muscle layers that can be seen in **Figure 2.1c**. The live organs are such complex physiological systems that everything can have a large effect on the drug or disease response.

While ex vivo tissues provide a much more physiological accurate model, there are several difficulties working with them. The first difficulty comes with the actual acquiring of the tissue, the dissection/preparation of the tissue is a very delicate process. Once the tissue is taken from its live host, it dies rapidly, so the time to place it in the device should be as little as possible. The tissue is also very sensitive so the middle section that is going to be examined after the experiment should not be touched by any tools. The second difficulty is tissue viability throughout the experiment. Current Ussing chamber experiments on live tissues have often been limited to under 5 hours [2], [11]. To develop better understanding of ex vivo models it is important to improve tissue viability. This allows longer experiments to be conducted after tissues have settled into their new environment inside the chamber. The third difficulty is the added diffusion layer resistance in tissues from the muscle and submucosa regions of the tissue. The electrical impedance

from these added diffusion layers can potentially overwhelm the electrical impedance of other layers, such as the mucosa layer, to study their permeability (see Section 2.5 for more details). The fourth difficulty is that all the equipment needs to be completely sterilized prior to an experiment. Live intestinal tissue has a lot of bacteria that comes with it, this means if the equipment is not sterilized then the chance of getting an infection is high. Despite all of the difficulties that come along with the ex vivo tissue, it is highly desirable to work with and develop ex vivo models for biomedical research [22]. To create a better ex vivo model, it is becoming clear that there needs to be improvements to Ussing chamber designs in terms of maintaining live tissue's viability, and easier application of TEER measurements with higher sensitivity and throughput,

2.4. Microfluidics and Appropriate Media Composition

As described in the previous section, creating better ex vivo models for epithelial transport processes and other organs is very advantageous in answering complex questions about the health and disease of organs in the body. The key to developing better ex vivo models is by using microfluidics and appropriate media composition [22]. It has already been widely shown that microfluidics in organ-on-a-chip (OoC) devices increased the viability of in vitro cell monolayers [9], [16], [17], [19], [20]. Microfluidics can also play a similar role for Ussing chambers with ex vivo tissue. The problem with traditional Ussing chambers is that they are devices with static media. In static cultures, the main concern is inadequate diffusion of oxygen and nutrients throughout the entirety of the tissue [22]. Attempts have been made to circulate media inside of the reservoirs by gas lift [2], this can potentially increase viability of the tissue but it also creates microenvironments that are uncontrolled [22]. To maintain tissue's viability for an extended period there needs to be a continuous media exchange through the microenvironment. Another benefit of microfluidics is the ability to simulate fluid flow and shear stress on the tissue. By combining the microfluidics of OoC devices with ex vivo tissue from the Ussing chamber, the researcher can have a much more physiologically relevant organ model that is able to stay viable for an extended period [26]. This allows for better insight into drug discovery and the tissues' overall health. Another important factor in increasing the viability of an ex vivo tissue is the use of appropriate media composition. The role of the media is to provide the tissue with nutrients to keep the tissue alive inside of its new microenvironment. Culture media should be optimized for amino acids, fatty acids, sugars, ions, cofactors, and vitamins to increase tissue viability [22]. When considering the GI tract specifically, researchers need to consider the oxygen gradient that is present. It has been previously discovered that low oxygen is required for better preservation of microbiota in the tissue [26], [27]. To create this oxygen gradient for the ex vivo intestinal tissue, mucosal media

is mixed with 0.5 M sodium sulfite to decrease oxygen levels and the serosal (muscle) media is kept at ambient oxygen levels. This experimental setup has proven to keep ex vivo murine intestinal pieces in a device viable up to 72 h.

2.5. Transepithelial Electrical Resistance (TEER)

2.5.1. Transepithelial Electrical Resistance

Transepithelial electrical resistance (TEER) is an electrical measurement of impedance of an epithelial barrier. More specifically it is a measure of the ion transport across an epithelial barrier. TEER is a widely accepted way of measuring the integrity of tight junction dynamics in epithelial barriers, this can then be directly correlated to the overall health of the barrier in question [10], [21]. Tight junctions are a collection of numerous protein complexes that create a leakproof seal in the epithelial, the healthier the barrier the "tighter" these junctions are. Tight junctions control a large part of the ion transport through the epithelial barrier. The junction tightness is directly reflected in its TEER values. Another reason TEER is a very useful parameter of barrier health is because it can be measured in real time and with little to no damage of the cells within the barrier. The alternative way to measure permeability of the epithelial barrier involves using fluorescently labeled tracers. However, the fluorescent methods can only be viewed after the tissue has been removed from the device. TEER measurements have evolved over the years as the need for better physiologically relevant epithelial barriers has increased. TEER-like measurements can be traced back to the first Ussing chamber [1], when Hans Ussing recorded the short circuit current I_{sc} across the dissected frog skin inside his chamber. Most modern experiments using TEER measurements are with in vitro cell cultures in either Transwell devices (see Section 2.3.1) or Organ-on-a-chip devices (see Section 2.3.2). There are two main methods of TEER measurement used today, Ohms Law method and impedance spectroscopy. These two methods will be described in detail next.

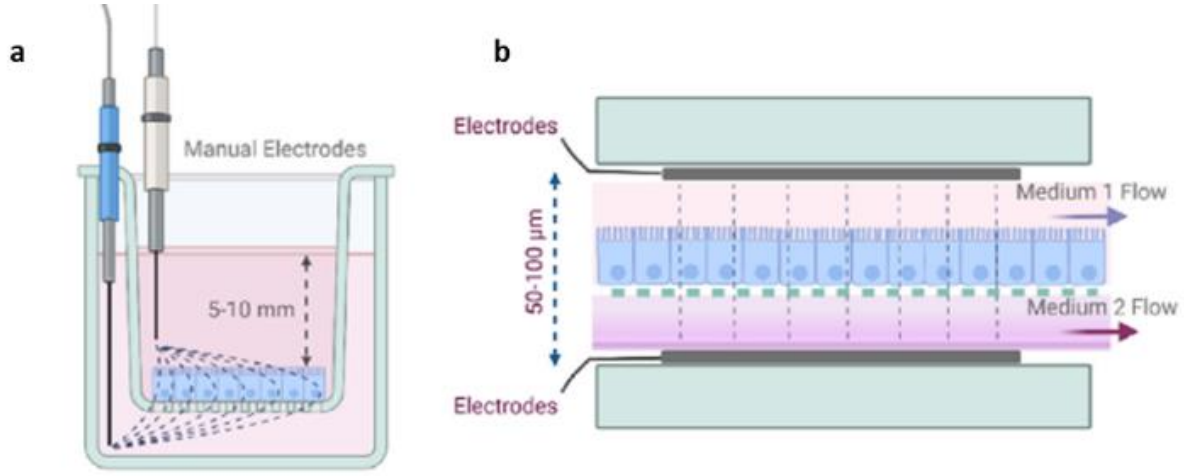

Figure 2.5: **a)** Electrode setup for Transwell experiment; **b)** Integrated electrode setup for OoC device, picture credit: [10]

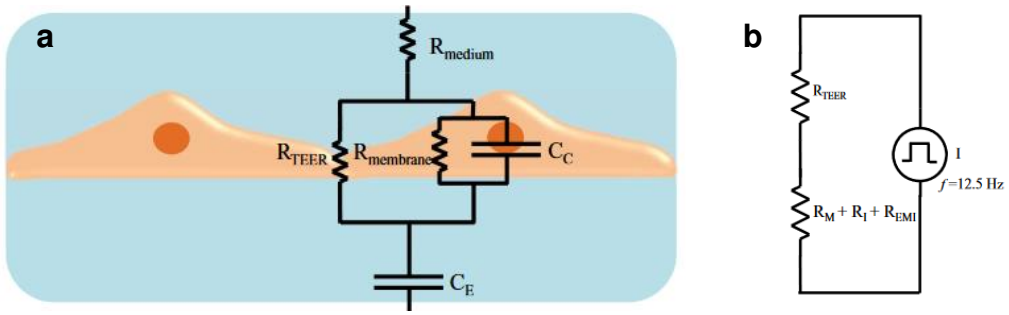

Figure 2.6: **a)** Full equivalent circuit diagram for epithelial barrier [21]; **b)** Equivalent circuit for Ohms law method [21]

2.5.2. Ohms Law Method

The Ohms Law method is a simple setup often used to obtain barrier integrity, such as those of a cellular monolayer [35]. To record the TEER value of an epithelial barrier using the Ohms Law method an electrode is placed on each side (apical and basolateral) of the barrier. The transwell system seen in **Figure 2.5a** is an example of how the Ohms Law measurement is setup. **Figure 2.6a** shows an equivalent circuit for the full measurement environment. The middle components, $R_{\text{TEER}}, R_{\text{membrane}},$ and C_C represent the actual physiological barrier (cell monolayer or tissue). The capacitance C_E and the resistance R_{medium} are parasitics associated with the measurement device. Component C_E is the double layer capacitance created from the electrode-media interface, and R_{medium} is the series resistance added from the media in the chamber. The traditional Ohms Law method would be performed by applying a DC voltage to one electrode and reading the resulting current through the cell barrier from the other. A problem with this is that DC

current can be harmful to the epithelial cells and the electrodes. The impedance of this equivalent circuit (**Figure 2.6a**) also can't be measure using purely DC voltages because of the series capacitance C_E. This series capacitance becomes an open circuit when a DC voltage is applied to it. To overcome these issues an AC square wave is applied instead. The high frequency transitions of the square wave eliminate the effects of all the capacitive elements in the measurement environment (**Figure 2.6a**) and allow the purely resistive components (**Figure 2.6b)** to be manifested and calculated. The resulting resistance can be calculated as the TEER using Eq. 2.1. Where R_{TEER} is the resistance of the cell layer, R_M is the resistance of the media, R_I is the resistance of the semi-permeable membrane insert, and R_{EMI} is the resistance of the electrode medium interface.

$$R_{\mathrm{TOTAL}} = R_{\mathrm{TEER}} + R_M + R_I + R_{\mathrm{EMI}} = \frac{V_{\mathrm{SQUARE}}}{I_{\mathrm{OUT}}} \qquad \textbf{(Eq. 2.1)}$$

To find the resistance of the epithelial barrier/tissue, R_{TEER}, the baseline measurement needs to be performed to obtain R_{BASELINE}. R_{BASELINE} can be found by performing the same measurement without the epithelial cell barrier in the well or chamber. By subtracting the R_{BASELINE} from R_{TOTAL} leaves the tissue resistance R_{TEER} (Eq. 2.2)

$$R_{\mathrm{TEER}} = R_{\mathrm{TOTAL}} - R_{\mathrm{BASELINE}} \qquad \textbf{(Eq. 2.2)}$$

The Ohms Law method is most widely used in commercial systems such as Epithelial Voltohmeter (EVOM; World Precision Instruments, Sarasota, FL) [9], [31]. The Ohms Law method of finding TEER has provided a good basis for understanding how TEER values can be used to quantify barrier integrity. However, this method does not fully represent the complete electrical impedance of the epithelial barrier. By using a single frequency AC square wave, the output TEER calculation is a representation of only the purely resistive components of the barrier. To find the true impedance of the barrier the electrodes need to be excited with a range of frequencies. This method is called electrical impedance spectroscopy.

2.5.3. Electrical Impedance Spectroscopy

Electrical impedance spectroscopy (EIS) is performed by applying an AC sinusoidal voltage stimulus signal across the targeting monolayer or tissue in a range of frequencies and then measuring the resulting amplitude and phase of the current signal. This allows researchers to categorize the epithelial barrier with an impedance spectrum. The impedance spectrum provides more information about monolayer or tissue's TEER values than the ohms law method. Many modern OoC and Ussing chamber devices have adopted the EIS method to measure TEER [3], [4], [7], [12],

[13], [16], [17], [20], [36]–[38]. Electrical impedance magnitude ($|Z|$) is calculated by dividing the peak voltage (V_0) of the stimulus by the peak current from the response (I_0) as shown in Eq. 2.3.

$$|Z| = \frac{V_{\mathrm{PEAK}}}{I_{\mathrm{PEAK}}} \quad \textbf{(Eq. 2.3)}$$

The phase shift (θ) between the voltage and current signals can be calculated by finding the time difference between peaks (t_{diff}) of the stimulus voltage and the response current as a percentage of the stimulus signal period (t_{period}) as shown in Eq. 2.4.

$$\boldsymbol{\theta}(deg) = 360° * \frac{t_{\mathrm{diff}}}{t_{\mathrm{period}}} \quad \textbf{(Eq. 2.4)}$$

The resulting magnitude, $|Z|$, and phase, θ, of the impedance Z can also be represented as a real (Z_R) and imaginary parts (Z_{Im}) of the impedance as shown in Eq. 2.5.

$$Z_R = |Z| * \cos(\theta)\,,\; Z_{Im} = |Z| * \sin(\theta)$$

$$Z = Z_R + jZ_{Im} \quad \textbf{(Eq. 2.5)}$$

Using EIS has allowed researchers to better understand cell monolayer or tissue's behavior as a function of frequency. There are several different sections of the epithelial barrier that influence its overall impedance. The epithelial barrier has two ion conductive pathways that make up the total TEER. These two paths are the paracellular (i.e., Between the cells) and transcellular (i.e., through the cells). Based on these two pathways, epithelia are put into two categories: first, when the TEER is low and has lower paracellular resistance, the epithelia is described as 'leaky'; second, when the TEER is much higher and the paracellular and transcellular resistances are similar then the epithelia is described as 'tight'. To better illustrate this, **Figure 2.7a** shows the two ion paths circuits where $\mathrm{R_P}$ represents the paracellular resistance. This resistance is due to the tight junction (TJ) protein connecting the cells. On the transcellular pathway, $\mathrm{C_a}$ and $\mathrm{C_b}$ represent the capacitance created from the apical and basolateral cell membranes; and $\mathrm{R_a}$ and $\mathrm{R_b}$ represent the ion permeability through the two cell membranes.

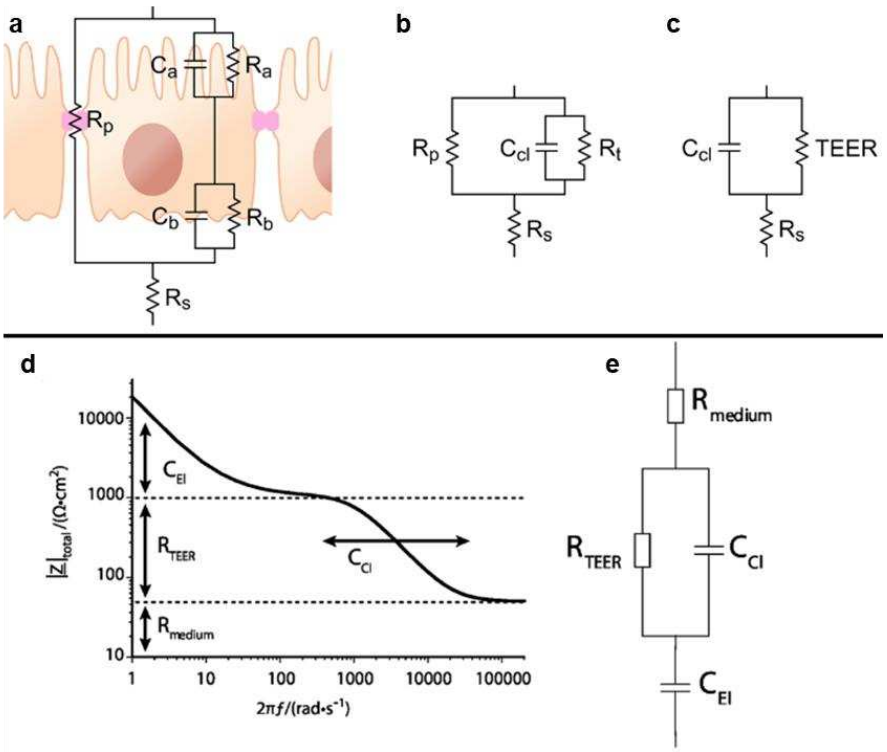

Figure 2.7: **a)** Full equivalent circuit for an epithelial layer [14]; **b)** First step in lumping elements, transcellular resistances lumped together [14]; **c)** Final simplified equivalent circuit, paracellular and transcellular resistances lumped together [14]; **d)** Impedance spectrum of circuit in (**e)** [21]; **e)** Equivalent circuit according to Srinivasan et al. [21]

Often, the components in **Figure 2.7a** are lumped together for simplicity as shown in **Figure 2.7b**, the transcellular resistances (R_a and R_b) and the transcellular capacitances (C_a and C_b) are combined into R_t and C_{cl}. The equivalent circuit in **Figure 2.7b** is often further simplified as shown in **Figure 2.7c**. The paracellular and transcellular resistances (R_p and R_t) are grouped together to represent a single resistance 'TEER' for the total ion permeability across the tissue. This final simplified equivalent circuit is the most common model used for calculating TEER using EIS. For completeness, Srinivasan et al. [21] added the media bulk resistance, R_{medium}, and the double layer capacitance from the electrode to media interface, C_{El}, into the simplified model as shown in **Figure 2.7e.** The impedance spectrum and the effect of each component can be seen in **Figure 2.7d.** The behavior of TEER in low frequencies is dominated by the double layer capacitance C_{El}. As the frequency increases, C_{El} eventually becomes shorted and the impedance spectrum levels out. The level it flattens out at is determined by the resistance of the tissue barrier (R_{TEER}) plus the resistance of the culture media (R_{medium}). As the frequency keeps increasing, eventually the cellular capacitance C_{Cl} becomes shorted, causing the impedance to slope down again. Finally, the impedance levels out at the resistance

R_{medium}. The mid-frequency range, between the regions dominated by C_{Cl} and R_{medium}, contains the important information about the TEER value. Like with the Ohms Law method, to find the true TEER value a baseline measurement needs to be subtracted away. For an EIS measurement this is done on a frequency-by-frequency basis.

2.6. Choice of Stimulus in EIS

Stimulus signals are very important to the accuracy and capability of any bioelectrical impedance measurement. There are two types of stimulus sources in any type of measurement, voltage source or current source. When electrical signals interact with biological cells and tissues, it is important that the electrical signals do not damage the target cells and tissues. In general, biological cells and tissues are very sensitive to the amount of current going through them. Using a voltage signal source for bioelectronic measurements can unintendedly increase amount of current going through the target cells and tissues if the magnitude of the stimulus voltage is not adapted to changing impedance, causing physical damages to the cells and tissues [39]. If there is no control over load value and no safety measure in place to lower input voltage, the current drawn can exceed the safety limit for the biological sample. For this reason, it is safer to use a current source input stimulus. The current source input ensures that there won't be large current spikes damaging the biological sample.

2.7. Howland Current Source

A common current source used for bioelectric applications is the Howland current source (HCS) [3], [39]. The HCS is a voltage controlled current source that can achieve high signal to noise ratio (SNR), high stability, and high output impedance [39]. The HCS schematic used can be seen in **Figure 2.8**. The key to the HCS topology is that the feedback networks from the output to the +, - input terminals are equal strength. This means that the resistive feedback networks are equal, seen in Eq. 2.6 and the current is set by the ratio between the voltage and the gain resistor R_3 Eq. 2.7.

$$\frac{R_4}{R_5} = \frac{R_3+R_2}{R_1} = 1 \qquad \textbf{(Eq. 2.6)}$$

$$I_{\text{out}} = \frac{V_{\text{in}}}{R_3} \qquad \textbf{(Eq. 2.7)}$$

By following these criteria, the output impedance can achieve a very high value. How high the output impedance reaches relies on the resistance matching of the two feedback paths. This can be intuitively realized with this simple scenario: first set the input voltage, V_{in}, to GND. As the load voltage (V_x) increases, a current is induced in resistors R_1 and R_2, (i_{pos}). The current i_{pos} then increases the positive input voltage (V_+) and assuming the op-amp is ideal,

then the negative input voltage (V_-) is equal to V_+. Now that $V_- \neq 0$, a current is induced in the negative feedback branch (i_{neg}) through resistors R_4 and R_5. Finally, the output voltage of the op-amp creates the current i_x through the resistor R_3. If the resistors satisfy Eq. 2.6, then the total currents going through each branch are equal. Making the circuit have an infinite output impedance. Small errors in the resistance values cause the output impedance to decrease drastically. To avoid this, the HCS circuit requires either very low tolerance resistors (<0.1%) or the use of resistor trimming. Another non-ideal component that can lower the output impedance (among other things) is the op-amp itself. The two most important specifications that should be considered for the HCS are the output swing and the CMRR. The output swing of the HCS is already going to be limited by the resistor R_3, so having an op-amp that can achieve rail-to-rail output is going to help minimize the total damage to the final output swing. CMMR is very important to reducing noise and keeping the two feedback branches close to equal, generally it is recommended that the CMRR should be over 80dB and as linear as possible [40]. Finally, a feedback capacitor over the negative feedback resistor can help with stability and filtering of high frequency noise.

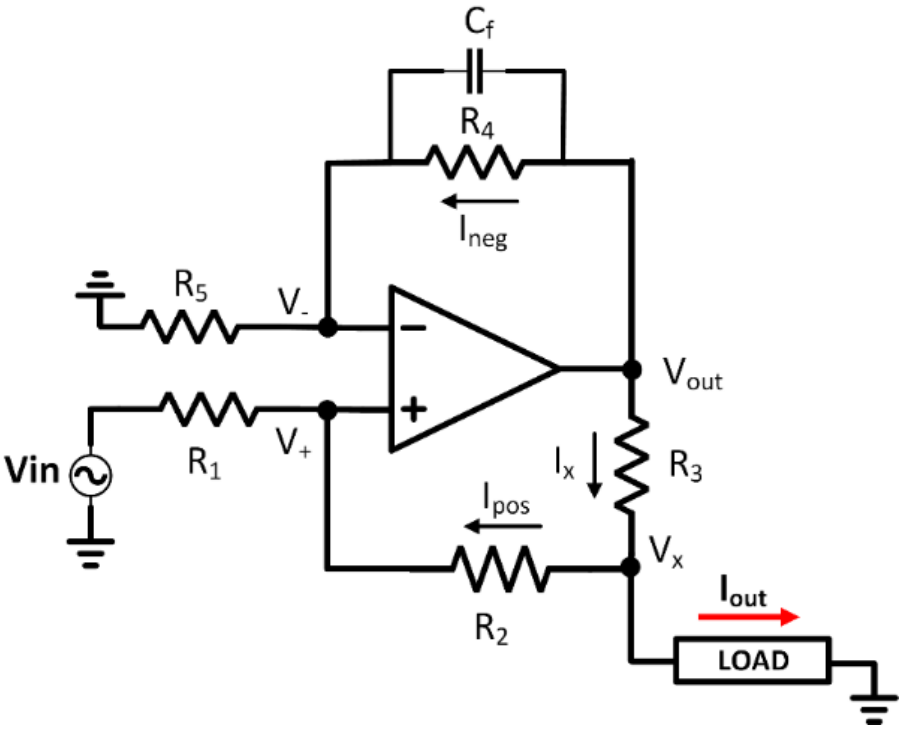

Figure 2.8: Howland circuit topology

Chapter 3 – Proposed System Design

3.1. Microfluidic Device Design

The microfluidic chamber (**Figure 3.1**) was designed using CAD (Autodesk, Inc) and fabricated using Anycubics UV sensitive resin and SLA printer. To avoid harmful effects from uncured resin, each chamber is fully cured using a lightbox and thoroughly rinsed with isopropyl alcohol. The chamber consists of two half chambers assembled to hold the tissues and make connections to the integrated TEER electrodes. Each half chamber is composed of the following (**Figure 3.1a**): the SLA printed chamber body; two 1mm thick PDMS layers for holding the electrode chip in place; one gold electrode chip; an aluminum clamp; and a printed circuit board (PCB) with spring headers that connect to the electrode chip. The fully assembled chamber (**Figure 3.1b)** consists of two halves, the top half has spikes to hold the tissue tight when the chamber is sealed. The bottom half is where the tissue is placed and spread out before closing the chamber. The tissue before and after the experiment can be seen in **Figure 3.1c**. There are holes in the bottom half to house the spikes from the top half chamber. During the closing of the chamber a 500µm PDMS layer is placed over the spikes of the top chamber (**Figure 3.1a**). This PDMS creates a flush seal against the tissue and prevents any leaks between the chamber halves. Tubing is connected to each chamber half through Luer lock connectors. Pictures of the actual assembled device (front and back respectively) can be seen in **Figure 3.1d** and **e**. Media is pumped into the chamber using custom-designed syringe pumps where users can specify start time and stop time points. With the tissue positioned over the circular opening between the chamber halves, a barrier is formed between the two media flows, one for the serosal side and the other for the luminal side of the tissue. The microfluidic path flows over the opening on each side exposing the tissue to the media composition. Providing balanced flow for the tissue inside the chamber is important for controlling shear stress and extending tissue viability [15], [22], [41]. 3D fluid simulations were performed to achieve the balance as much as possible. **Figure 3.2** is a flow simulation using CFD, this was used to ensure the flow of media is uniform over the top of the tissue.

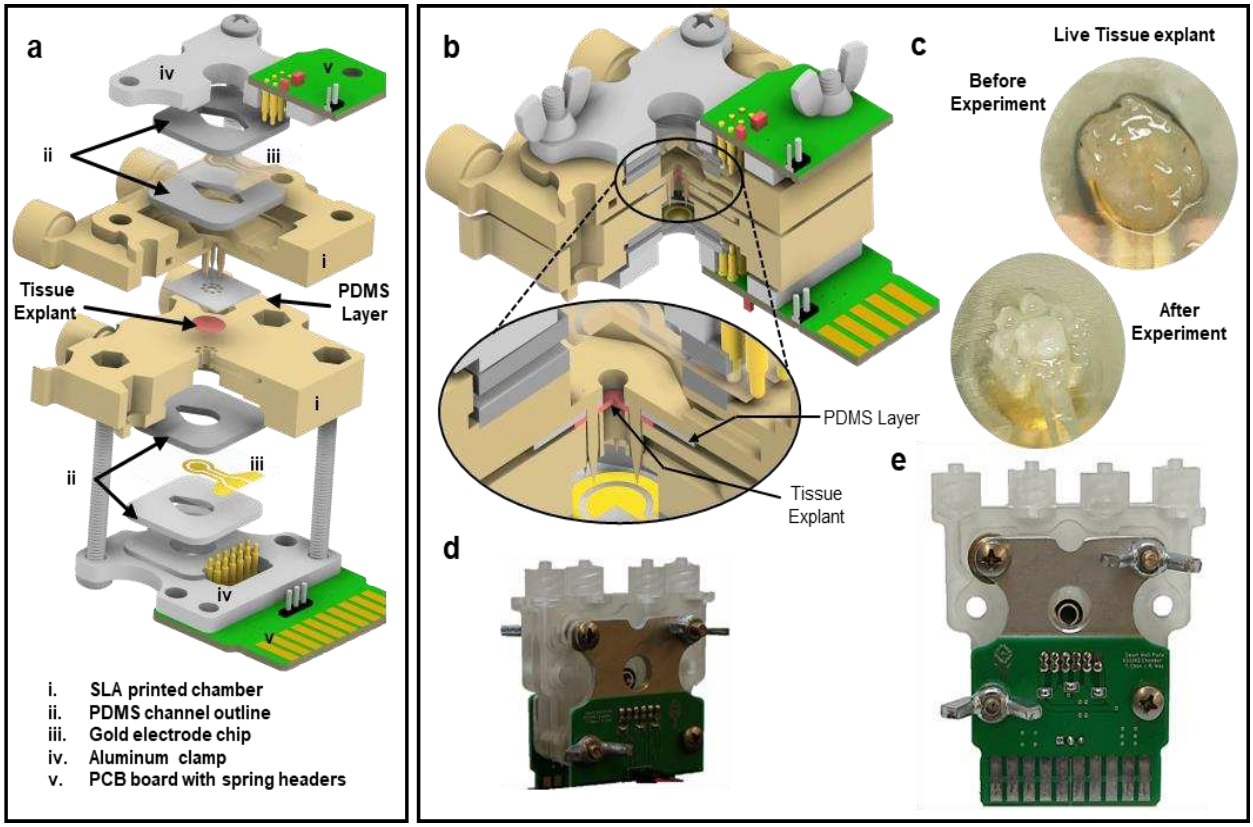

Figure 3.1: Single Microfluidic Chamber Design. **a)** Expanded view of a full chamber, with all components labelled. **b)** Closed chamber with a closeup view of the tissue and PDMS clamped between two chamber halves. **c)** Picture of real tissue explant before and after the experiment. **d** and **e)** Photos of the actual chamber assembled (front and back respectively).

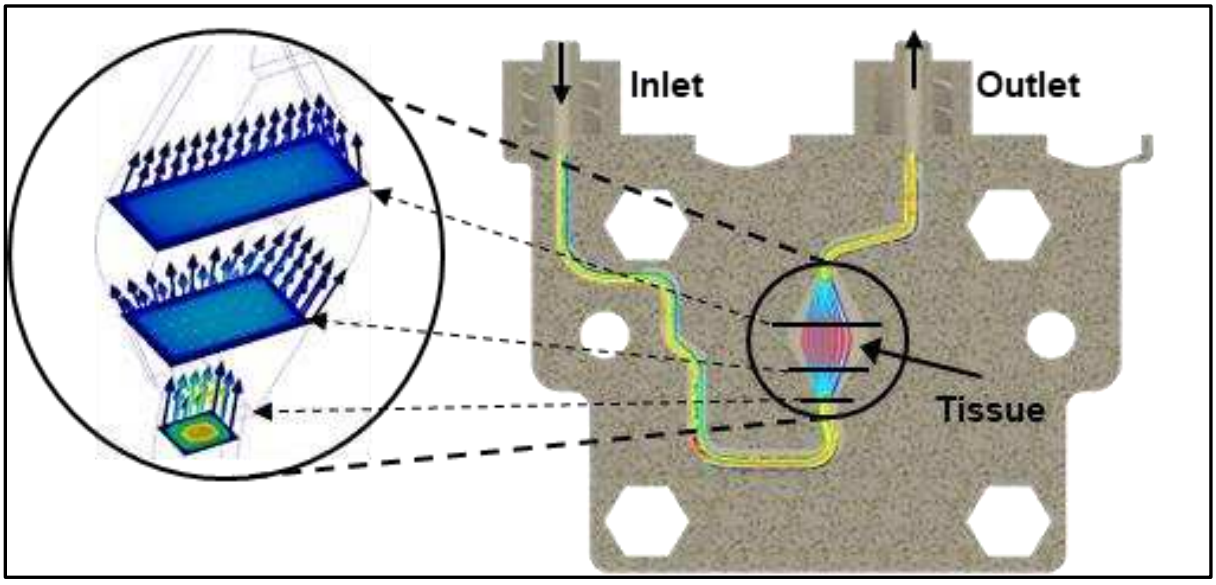

Figure 3.2: Flow simulation using CFD software. The right picture shows the full media flow path through the microfluidic channels and the zoomed in view shows the flow pattern through three planes in the path over the tissue opening.

Each chamber half has its own PCB board that connects to the electrode chip through gold spring headers. The top half chamber has wires connecting to the bottom halves PCB and the bottom PCB includes a card edge connector that is plugged into the microphysiological system (*see section: "System Overview")*. The chamber, when plugged in, is oriented so that the media inlet is pumped into the bottom and flows out the top. This is helpful because if an air bubble forms, it is likely to float to the top and be pushed out of the media outlet. Air bubbles can injure the tissue, and cause problems for the TEER measurement.

3.2. System Overview

The entire system is housed in a shield box (**Figure 3.3a** and **b**). The box has power and USB ports for connecting it to a host computer. All electronics for performing TEER measurement are housed in the box. The microfluidic chambers are plugged into the card edge connectors at the top of the box after the tissue has been loaded into the device. The connectors on the microfluidic chambers and the box are all universal, allowing for plug-and-play functionality. The current system can hold up to three chambers at a time. All PCBs inside of the box are custom designed to achieve the compact size necessary to fix the entire system into a limited environment chamber space during experiments **Figure 3.4a**. The electronics inside of the box are responsible for performing the TEER measurement and are controlled by an FTDI-based microcontroller via the USB port. A custom graphic user interface

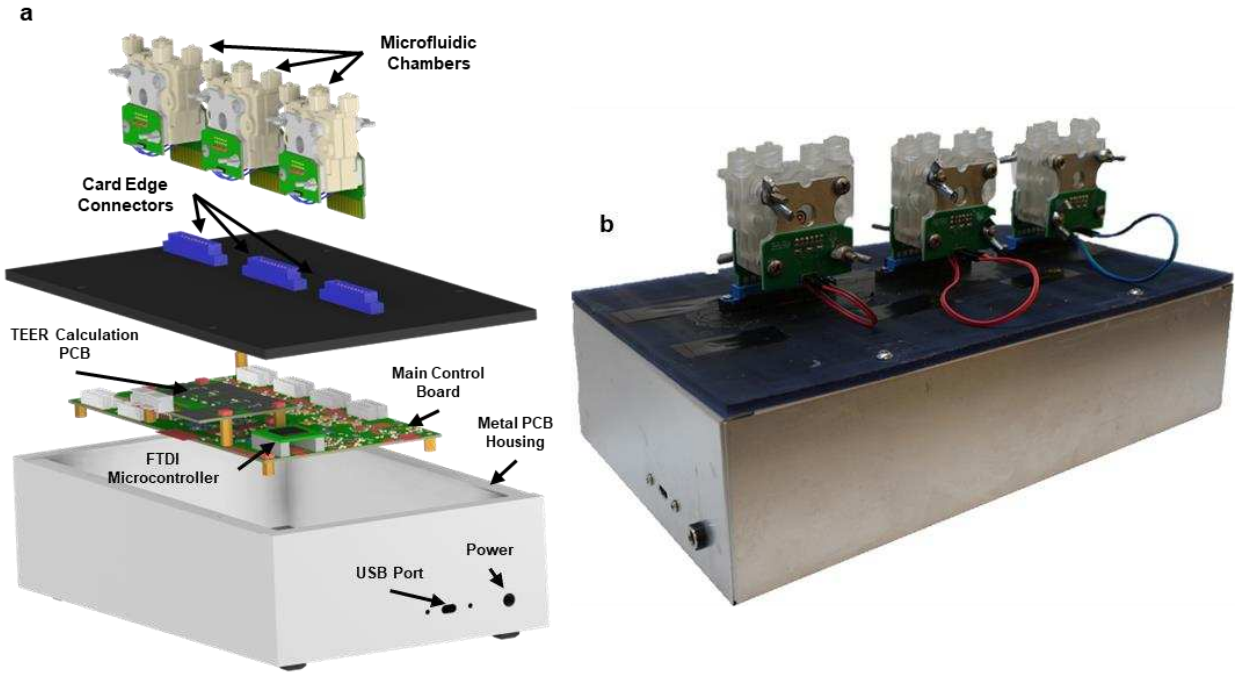

Figure 3.3: a) Full system design including electronics housing and microfluidic chambers. **b)** Actual box used in experiments

(GUI) was designed to allow user configurations for the experiment **Figure 3.4b**. The measurement data from the experiment is acquired via the USB port and is saved on the host computer.

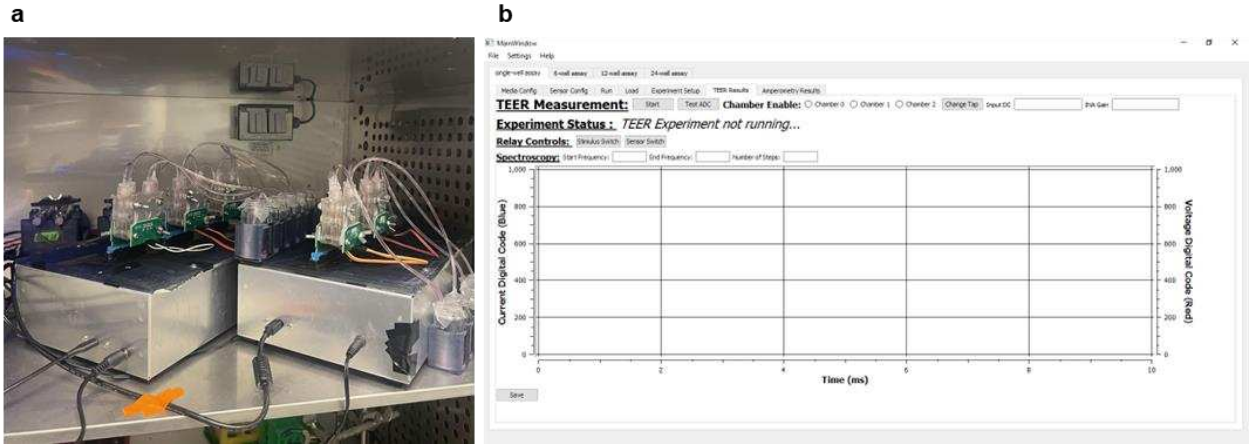

Figure 3.4: a) Experiment setup with two boxes running side by side inside of the incubator. **b)** GUI experiment page

The electronics consist of two main PCB boards: the main control board, responsible for the power supply, microcontroller, ADC, signal generator, and more; and the TEER calculation board, which holds the circuitry responsible for performing the TEER measurement and connecting to the microfluidic chamber's electrodes. The full system bock diagram, showing the flow of signal conditioning and processing can be seen in **Figure 3.5**.

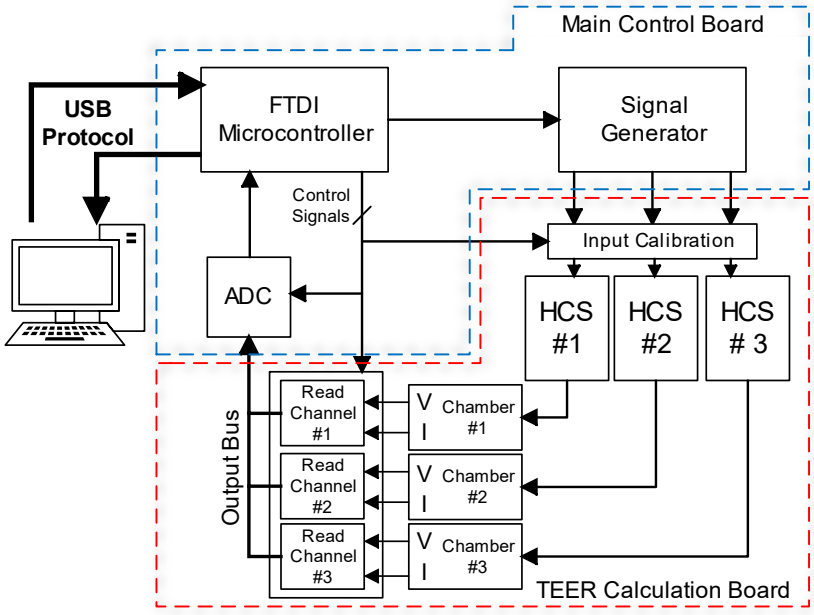

Figure 3.5: Full system flow diagram

3.3. Main Control Board Design

The main control board (**Figure 3.6**) inside of the metal housing was designed to be the brains of the entire system. The control board is composed of several crucial design blocks. These include power supply circuitry, microcontroller, signal generator and ADC, control signal circuitry, and metabolic measurement instrumentation. Metabolic instrumentation is circuitry that is used in a separate project in our lab. Future design plans have the two projects merging, so all electronics can be housed in a single device. This thesis does not involve the use of this circuitry.

The entire system is powered by a 9V DC signal. To distribute the power throughout the board, the initial DC signal is divided into four separate DC signals using adjustable low-dropout (LDO) voltage regulators. Two of the voltage regulators are adjusted to output a voltage of 5.5V and are responsible for powering the Texas Instruments LM27762EVM positive and negative output charge pump evaluation boards. These evaluations boards supply the main ±5V power supplies to the rest of the circuit. To ensure the system does not draw too much current, the power supply is split into two separate regions. Powering only enough components to not draw too much power. The boards are then fastened to the main PCB using spacers. The use of evaluation boards for the power supply saves space on the main control board and allows for simple installation. The third voltage regulator is used to power all the relay switches in the system. The relay switches draw a lot of power compared to all other components. For this reason, they were given their own power supply to ensure they don't draw too much power and negatively affect any of the other circuitry. The final power region controls all the digital electronics on the board. This includes the analog to digital converter (ADC) and the signal generators. The digital electronics require a lower voltage power supply of 3.3V because it is an unnecessary waste of power to keep digital signals on the analog power supply.

The microcontroller used for the system is FTDI's FT2232H Mini Module evaluation board. It is connected to the main control board through two 26-pin female headers. The reason for this is the same as the power evaluation boards, it saves space on the main board, and allows for easy installation. The FT2232 chip is a dual channel Multi-Protocol Synchronous Serial Engine (MPSSE) USB interface device. Both channels were configured to SPI serial communication. The SPI channels handle all control signals, control the signal generator output, and receive the digital output from the ADC.

The signal generator and ADC chips are located in the digital electronics region because they communicate to the FTDI through a 3.3V digital signal. There are three separate signal generators on the board that can all be operated in

parallel. These are used to generate the stimulus signals used during an experiment. The signal generators used are AD9833 direct digital synthesis (DDS) chips. The AD9833 is capable of providing sine, square, and triangular waves with a frequency range of 0 to 12.5MHz. The ADC used in this device is MAX11192, which offers dual simultaneous sampling and a resolution of 12 bits. To increase the common mode rejection and resolution, the input signal to the ADC is differential. This is done by sending the signal through a single-ended to differential conversion circuit. To reduce the amount of error from this conversion, high precision resistors (<0.5% tolerance) were used to ensure equal gain for both positive and negative signals.

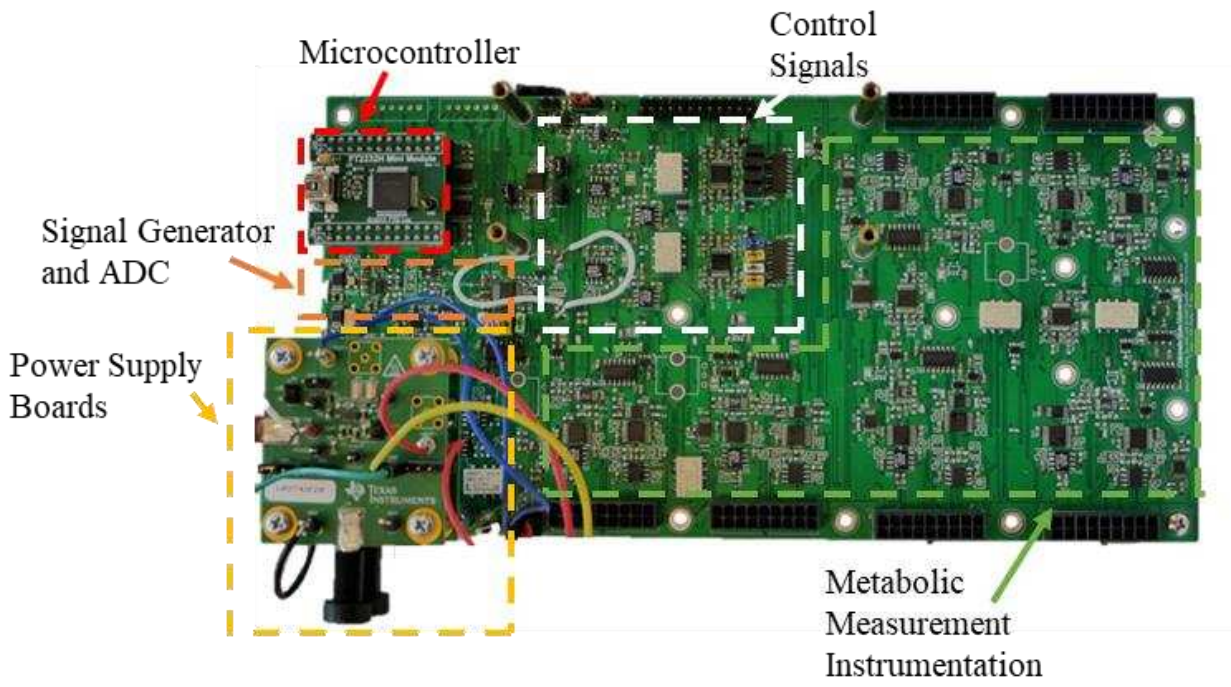

Figure 3.6: Main Control Board PCB

3.4. TEER calculation board

The TEER calculation board is a separate smaller PCB that is mounted to the main control board through metal spacers (**Figure 3.7**). All signals needed are then wired up from the main board. The TEER calculation circuit contains an input stimulus level shifter, Howland current source (HCS), and read channels that directly connect to the electrodes from the microfluidic chamber. The full system is capable of running three microfluidic chambers at a single time. Each microfluidic chamber requires its own separate TEER calculation circuit (level shifter, HCS, and read channels).

Output signals from the read channels are then all connected to a single bus that feeds into the ADC. The output signal is selected by the control signals from the main control board.

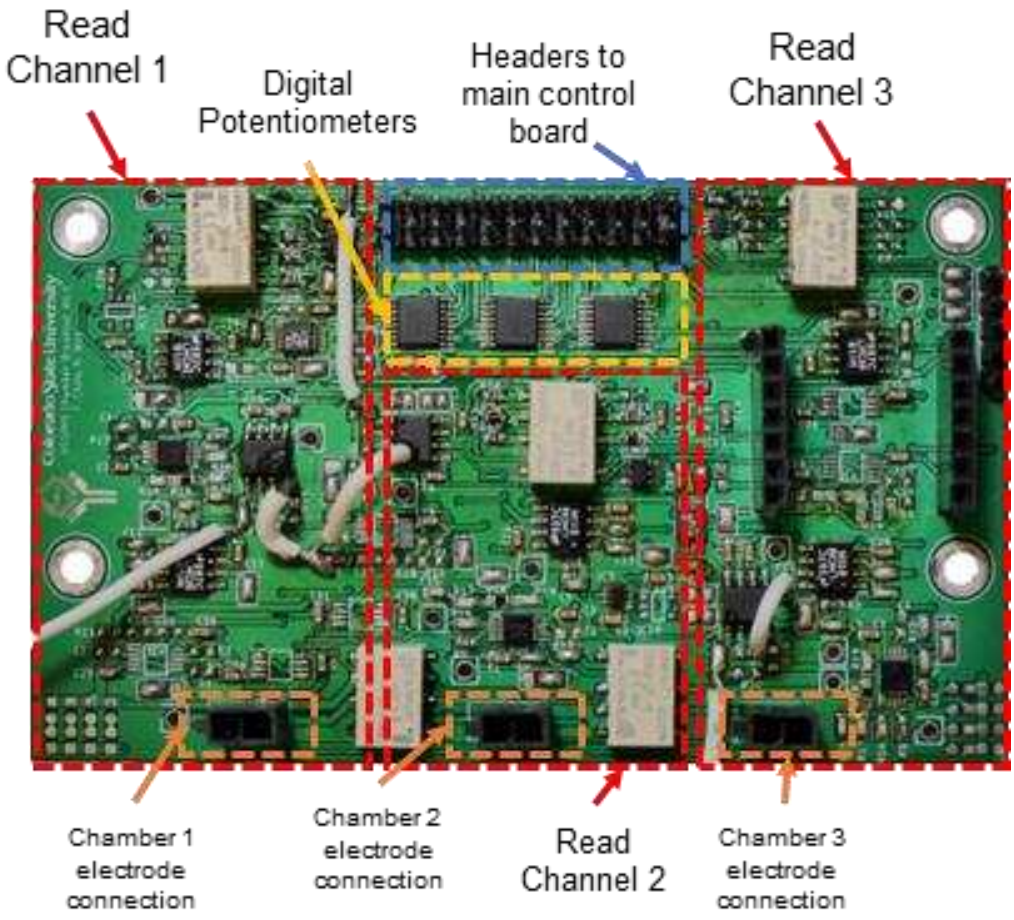

Figure 3.7: TEER calculation board

The input level shifter (**Figure 3.8**) is responsible for constructing the input stimulus signal that will determine the output current from the HCS. The input voltage comes directly from the AD9833 signal generator on the main control board, which has a constant amplitude and DC shift of 306mV and 344mV respectively. To be able to customize the output current from the HCS the input level shifter has a relay switch to select the voltage gain resistor and a digital potentiometer to control the DC voltage. The voltage gain is divided into two categories, high and low. The high gain will result in a high output current, and the low gain will result in a low current. This greatly increases the range of impedances that can be measured with this device. When the current is too high, a high impedance load will make the output voltage rail, producing a false calculation. The current selected is fully customizable by the user through the

GUI, allowing the experiment to be configured to many different scenarios. The DC voltage of the output is controlled by a digital potentiometer. The output voltage is designed to be as close to 0V as possible. This is because any DC shift on the input to the HCS is translated into DC current sent to the chamber electrodes. DC current is physically harmful to the biological sample and causes many problems for reading output voltage (discussed more in section: "*TEER Calculation*"). To minimize the DC offset from the input level shifter, the digital potentiometer performs a calibration algorithm using the binary search method, to find the smallest amount of DC offset possible. The calibration algorithm is run before every measurement.

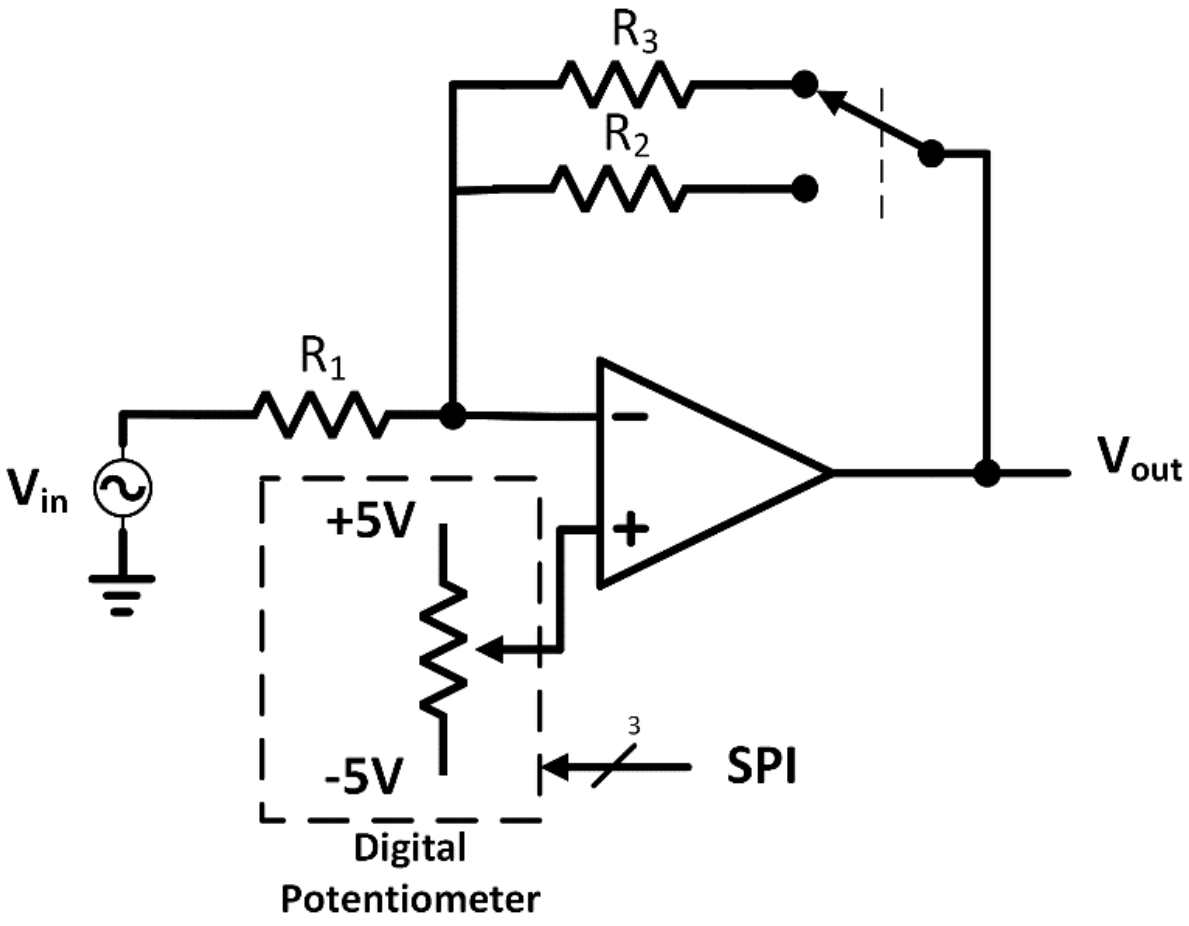

Figure 3.8: Input level shifter circuit

The HCS, read channels, and electrode interface can be seen in **Figure 3.9a**. The HCS circuit (see section 2.7) provides the AC current stimulus signal directly to the input current electrode and is controlled by the input voltage signal from the input level shifter. The LTC2052 was chosen for the operational amplifier (op-amp) because of its low offset

voltage (3μV), rail-to-rail output voltage, and high CMRR. The output current settings are 75μA, 5μA amplitude sine waves, and a 50μA amplitude square wave. These values are set by both the input voltage amplitude and the HCS gain resistors value, which is 50kΩ in this case. The HCS uses high precision resistors (<0.1%) to achieve high output impedance. The HCS also employs a feedback capacitor in the negative feedback loop to help with stability and filtering.

The microfluidic chamber includes four gold electrodes (two on each side of the barrier) for measuring the current and voltage across a biological sample. The electrodes on each side are for current and voltage separately. The resulting current and voltage signals are then used to calculate the impedance of the biological sample. Across the microfluidic chamber there is a relay switch in parallel. This relay switch is used to bypass the biological load entirely, so that in between measurements, there is no current flowing through the tissue or electrodes. Another reason for this is that it discharges any built-up charge on the input current electrode. The HCS always has a small amount of DC current, this DC current eventually builds up charge on the input electrode and changes its DC voltage. The input electrodes build up charge because they create a series capacitance in the equivalent circuit (see section 2.5). The relay switch is able to "refresh" the electrodes so that this extra charge doesn't rail the output voltage reading because of too much DC voltage.

The read channels for the TEER measurement circuit are what read the voltage and current signals from the load impedance. The output current signal is read by a transimpedance amplifier (TIA). LMC6081 is used because of its ultra-low bias current (10fA). The gain of the TIA is set to 27,000x by the resistor R_{gain}. In parallel with the resistor R_{gain} is a compensation capacitor C_c to filter out any high frequency noise and help stability. The voltage output is ready by the instrumentation amplifier (INA), AD8221BRZ. A single resistor R_g is used to set the gain of the INA, for the majority of the experiments this value was set to 9.8214x. Both output voltage and current are then individually output onto the bus (V_{bus}) through unity gain voltage buffers. The LTC2052 is also used for the voltage buffer because of its dual package and individual disable pins for each op-amp. The op-amps when disabled are put into a high impedance output state, allowing for the bus signal V_{bus} to be driven by as many op-amps as needed.

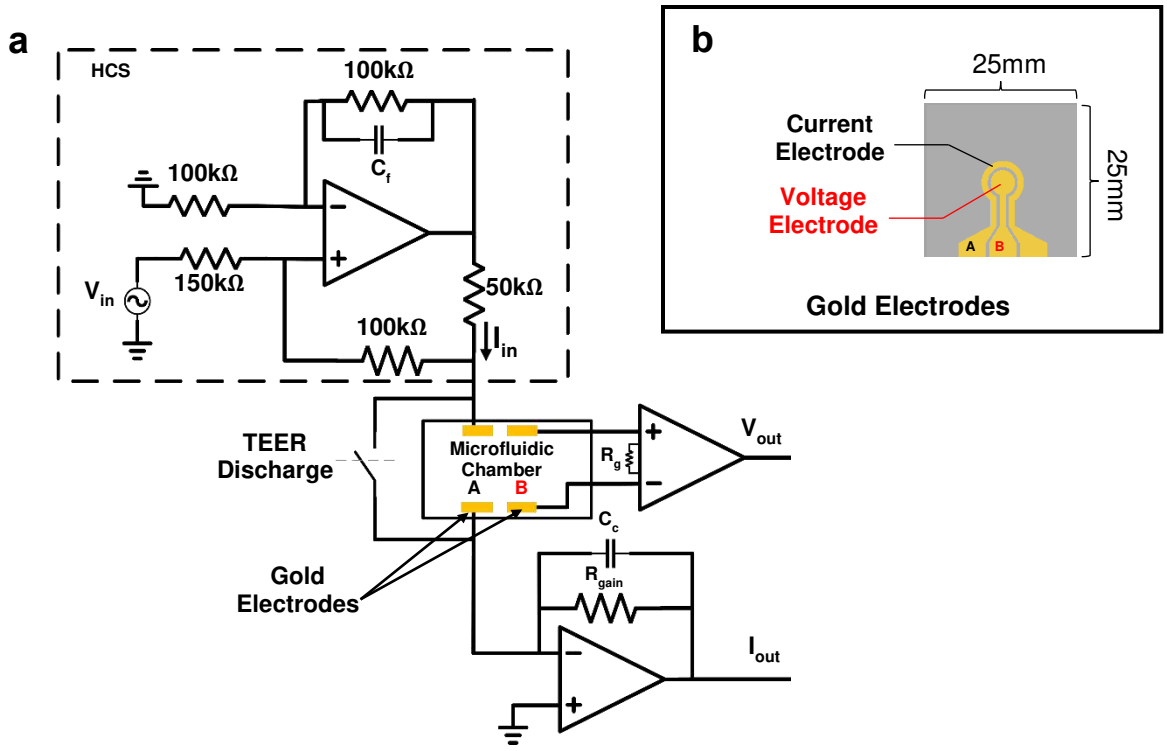

Figure 3.9: **a)** Howland current source and read channel circuits for each microfluidic chamber. **b)** Gold Electrode Chip on a 25mm x 25mm glass substrate. The outer ring is the current electrode, and the middle circle is the voltage electrode. The rectangular pads at the bottom are used to connect to the spring pins, using copper tape wrapped to the back.

3.5. USB Interface Software

To control the flow of information and perform the experiments, the system utilizes a USB interface capable microcontroller (MCU) from FTDI. This MCU has two Multi-Protocol Synchronous Serial Engine (MPSSE) channels that were configured to use SPI interface. This chip also has general purpose input/output (GPIO) pins that are used for digital control pins throughout the board. Finally, a GUI was developed using C++ in Qt software, to allow the user to customize experiment configurations and perform different types of tests.

The SPI interfaces from the MCU are responsible for controlling several different digital components throughout the system. These components include signal generators, the ADC, digital potentiometers, and a GPIO expander. The SPI interface is a simple and fast communication method to control these digital components in real time.

GPIO pins are one-bit digital outputs that can be controlled in real time by software. These are used as control signals for the entire system. This includes different multiplexers and other digital logic, as well as the ADC bus signal. All sensor readings throughout the system have to be sent through the ADC before being transferred to the host computer.

This is done by having a single bus that leads into the ADC and a buffer network that allows one signal through at a time. The GPIO pins control three separate decoders that can turn on and off the voltage buffers for the bus. By doing this, fewer GPIO pins are required to control the same number of voltage buffers. The GPIO pins also require to be level shifted because the decoders require ±5V control signals. This is another reason to use fewer GPIO pins for buffer control.

The GUI was designed to create a user-friendly interface that allows the user to run an experiment with this device. To start the experiment, the user presses the start button, and the status of the experiment is displayed on the screen. The software will then run continuously, taking a measurement every two hours, until it is stopped. The TEER data is automatically saved to the host computer after each measurement. Most of the experiment customization is done inside of the code, making the current GUI, a working prototype that can be improved upon in future iterations of the project. The majority of the experiment features can easily be adapted to be customizable in the GUI interface (section 5.2.7).

3.6. Electrode Design and Manufacturing

The electrodes are manufactured in gold on a glass substrate. Each electrode chip consists of two gold (Au) electrodes, a current electrode to supply (or read) the constant current signal from the HCS, and a voltage electrode to read the resulting voltage across the tissue barrier (**Figure 3.9b**). The electrode chip was fabricated on a 25mm x 25mm glass substrate through standard photolithography and lift-off techniques. The mask was designed using AutoCAD software (Autodesk, Inc.) and manufactured by Artnet Pro (San Jose, CA). **Figure 3.9b** shows the electrodes on the 25mm x 25mm glass substrate. The full photolithography steps are described in previous work [42].

3.7. Chamber Sterilization

To prevent infection during experiments, all components of the microfluidic chamber (chamber body, glass electrode chip, PDMS layers, PCBs, tubing, and Luer locks) were put through the first round of sterilization protocol:

1. 20-minute bath in 1:10 bleach to water ratio.
2. 10-minute soapy water bath inside of ultrasonic cleaner.
3. Next, thoroughly rinse with DI water.
4. 45-minute bath in 70% ethanol.
5. Finally, thoroughly rinse with DI water and let air dry.

After the first round of sterilization, the chamber was fully assembled with metal screws and clamps that have been autoclaved (30-minute, gravity cycle). After all chambers are assembled, the chambers went through low temp gas sterilization and are kept in a sealed bag until the experiment starts.

3.8. Animals, Tissue Collection, and Media Preparation

In all experiments, male C57BL/6 background mice aged 3-4 months were used. Mice were kept on a 12-h light/dark cycle with access to standard chow and water ad libitum. Animal protocols were approved by the Institutional Animal Care and Use Committee (IACUC) at Colorado State University under United States Department of Agriculture (USDA) guidelines.

Mice were deeply anesthetized with isoflurane and terminated via decapitation to prepare for tissue collection. The intestines were removed and immediately placed in 4°C 1x Krebs buffer (in mM: 2.5 KCl, 2.5 CaCl2, 126 NaCl, 1.2 MgCl2, 1.2 NaH2PO4). To prevent contractions during dissection, the Krebs buffer contained 1µl/1mL1mM nicardipine (Sigma Aldrich, St. Louis, MO), an L-type calcium ion channel blocker. Colon was then dissected to remove any remaining mesentery. For experiments in which muscle was removed, a 26G needle was used to gently tease away the muscle layer on the mesenteric edge of the tissue. Tissue was then cut longitudinally using angled vascular scissors to form flat pieces of tissue around ~5mm.

Adult Neurobasal media was custom made in house with 2% B27 supplement (Thermo Fisher scientific, Waltham, WA), 4mM glucose, 3% 1 M HEPES buffer (Sigma Aldrich, St. Louis, MO), without phenol red. To help maintain the gut microbiome, luminal media contained 0.4 mg/ml inulin (soluble fiber) and 0.5 M sodium sulfite (oxygen scavenger) to decrease oxygen levels [26]. The serosal media had ambient levels of oxygen creating an oxygen gradient across the tissue which we previously demonstrated [27] is necessary for preservation of a physiologically relevant bacterial community. After 24 h, luminal media for control tissue was not changed. Treatment group luminal media contained 5.80*10-2 U of broad spectrum bacterially sourced collagenase (Worthington Biochemical, Lakewood, NJ) or was treated with hydrochloric acid (HCl) to acidify the pH to 2. After completion of experiments, 0.05 M phosphate buffered saline (PBS) containing 0.5% cetylpyridinium chloride (CPC) was gently pipetted onto the tissue to preserve the mucus layer. The tissue was then gently removed from the device and placed in 4% paraformaldehyde (PFA) containing 0.5% CPC at 4°C for 24 h. Tissue was stored in PBS at 4°C until sectioning.

3.9. Tissue Sectioning and Histochemistry

Detailed methodology can be found in our previous publication [26]. Briefly, 1-3 mm sections of colon were submerged in agarose until polymerization. Tissue was then cut on a vibrating microtome (VT100S; Leica microsystems, Wetzlar, Germany) at a thickness of 50 µm. For lectin and immunohistochemistry, sections were first washed in 1x PBS, then incubated in 0.1M glycine followed by PBS washes and incubated in 0.5% sodium borohydride followed by PBS washes. Sections were then blocked in PBS with 5% normal goat serum (NGS; Lampire Biological, Pipersville, PA), 1% hydrogen peroxide, and 0.3% Triton X (TX). Next, sections were placed in PBS containing 0.3% TX and 5% NGS with the appropriate lectin or antibody for 2 days. The lectin used was Ulex Europaeus Agglutinin I conjugated to Rhodamine (UEA-1; Vec-tor Labs) at a concentration of 0.125µg/mL. The primary antibodies used were anti-claudin1 (Invitrogen) 1:200 and anti-peripherin (Sigma-Aldrich) 1:300. After lectin or primary antibody incubation, sections were washed in PBS with 1% NGS. Sections incubated in primary antibody were then incubated with PBS containing 0.02% TX and Alexa Fluor 594 conjugated to secondary antibodies specific to the species of the primary anti-bodies at a 1:500 dilution. Finally, sections were washed in PBS, mounted on slides, and cover slipped. Images were taken using an Olympus BX61 equipped for epifluorescence imaging or a Zeiss LSM800 upright confocal laser scanning microscope and a 20x (W Plan-Apochromat 20X/1.0 DIC Vis-ir ∞ /0.17) objective.

3.10. TEER Calculation

Calculation of TEER values involve filtering and conditioning to reduce noise and other artifacts before applying a curve fitting algorithm to obtain the magnitude and phase the voltage and current. The impedance magnitude ($|Z|$) and phase difference (θ_{diff}) can then be calculated using Eqs. (3.1) and (3.2). Where Av_{current} and Av_{voltage} are the current and voltage gain values respectively.

$$|Z| = \frac{V_{\text{peak}}}{I_{\text{peak}}} * \frac{Av_{\text{current}}}{Av_{\text{voltage}}} \qquad \textbf{(Eq. 3.1)}$$

$$\theta_{\text{diff}} = \theta_{\text{voltage}}(\text{deg}) - \theta_{\text{current}}(\text{deg}) \textbf{ (Eq. 3.2)}$$

The magnitude and phase values are calculated for each frequency to obtain the impedance spectrum of the tissue sample, commonly referred to as “electrical impedance spectroscopy (EIS)” Due to its versatility of revealing impedance information across a wide range of frequencies, EIS is a widely-used technique to discover the impedance

characteristics of tissue samples in Ussing Chambers and Organ-on-a-chip devices [3], [4], [7], [12], [13], [16], [17], [20], [36]–[38].

The sinusoidal curve fitting is necessary to further reduce noise and unwanted artifacts in the acquired TEER signal as it is illustrated in **Figure 3.10**. The smoothed signal can provide more accurate magnitude and phase values for the subsequent TEER calculation **Figure 3.10a**. The curve fitting algorithm also provides drifting correction to the acquired voltage response signal. Drifting of the response voltage signal is caused by offset DC current from the Howland circuit. This offset DC current builds up charge on the serial capacitance associated with electrode's double layer capacitor, resulting in a constant rate increasing (or decreasing) of the DC voltage at the voltage electrodes from the chamber. This effect can be seen in **Figure 3.10b**. The time dependent DC shift of the sinusoidal signal in **Figure 3.10b** needs to be leveled before the sinusoidal curve fitting algorithm can be applied to obtain its magnitude and phase. This is done by subtracting a 1st-order polynomial function from the acquired (drifted) voltage signal as illustrated in **Figure 3.10c**.

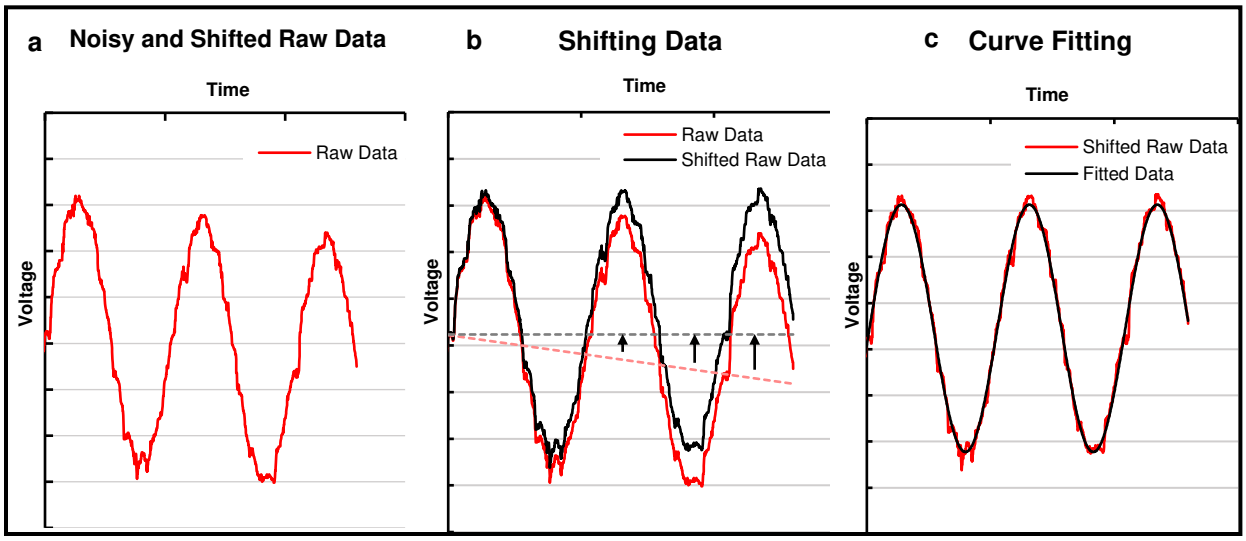

Figure 3.10: Curve fitting algorithm example. **a)** The fitted signal (black) removes all the unwanted artifacts from the acquired signal (red). **b)** Acquired voltage signal drifts over time due to the offset DC current signal from HCS. **c)** An example illustrating the drift correction performed by the fitting algorithm. The 1st degree polynomial (dotted red) of the input data is subtracted point by point from the input raw data (solid red), effectively flattening it out. Once the input data is flattened out it can be fit to a sinusoidal curve (black) using the curve fitting algorithm in part a.

The TEER value of an epithelial barrier is the resistance of the transcellular and paracellular combined. However, the TEER values obtained from Eqs. (3.1) and (3.2) contain the electrode double-layer capacitance and the media bulk resistance (see section 2.5)[21], [35], [37]. In order to obtain the actual TEER values associated with the epithelial barrier, baseline TEER measurements were performed for each experiment to capture the medial bulk resistance. The

final TEER value of interest was obtained by subtracting the baseline TEER values from the measured TEER values. It should also be noted that the magnitude $|Z|$ used for TEER measurements should be at an appropriate frequency not too low to reduce the effects of electrode double-layer capacitance, but not too high where the epithelial layer is shorted by its parallel capacitance, this can be deduced from the equivalent circuit of the epithelial barrier[35]. From the impedance spectrum of the tissue measured with this device, it was found that this value is at 5kHz.

The TEER value can also be calculated by finding the DC response from a square wave. Since the microfluidic chamber system is also capable of producing a square wave stimulus signal, the TEER using the ohms law method was also calculated. This value shows the pure resistance of the tissue barrier. **Figure 3.11a** shows a set of TEER values obtained using a 5kHz sinusoidal stimulus vs. a square wave stimulus. It was found that the TEER values obtained using the square waveform are lower (7.2% on average, $n = 10$) than those obtained using the 5kHz sinusoidal waveform by a constant margin. This is due to the fact that the relatively fast transitions in the square waveform stimulus were able to significantly reduce the effect of the double layer capacitance associated with the electrodes on TEER magnitudes compare to that from the 5kHz sinusoidal stimulus. If the sinusoidal stimulus frequency is decreased, then the effect of the double layer capacitance is more pronounced, making the TEER value increase as the input frequency decreases. **Figure 3.11b** confirms this by showing the percent difference between the sinusoidal and square wave increases as the frequency decreases. When the stimulus frequency reaches 3kHz and

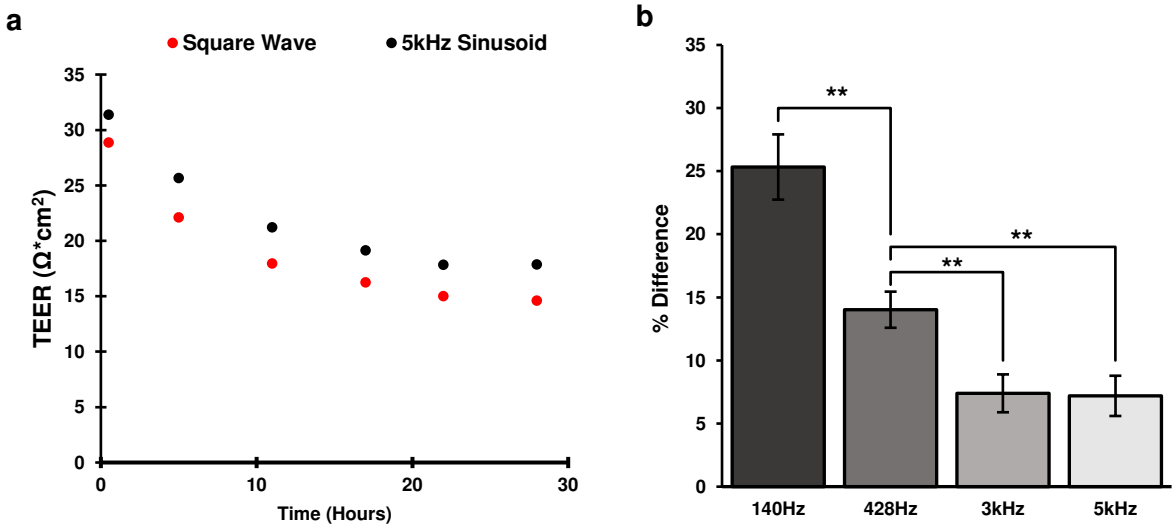

Figure 3.11: TEER calculated using ohms law method vs. using sinusoidal stimulus signal. Both measurements were using the same tissue, chamber and taken one right after the other. **a)** Example of a single tissue measured with square wave and 5kHz sinusoidal stimulus signals. The square wave stimulus is consistently lower than the sinusoidal value. **b)** The average difference between sinusoidal and square wave TEER calculations for different frequencies. The values presented in the b, n = 10, **: $P < 0.005$.

above, the difference between sinusoidal and square wave data flattens out. This is evidence that the stimulus frequency is now high enough to bypass the double layer capacitance. This is further validation that the choice of 5kHz sinusoidal stimulus was appropriate for the TEER measurements.

3.11. Experiment and Measurement Procedure

After all tissue slices are cut and prepared according to Section *Animals, Tissue Collection, and Media Preparation*, the explants were then loaded into the microfluidic chamber, one by one. First, the explants were placed on the bottom half chamber and then gently flattened out using forceps, careful not to touch the luminal side and damage the mucosa. After the tissue was flattened and centered over the hole on the bottom half chamber, the top chamber was slid down the metal screw guides to secure the tissue in place and create a tight seal. The chamber was then tightened using wing nuts and inserted into the card edge connector on the box. Next the inlet and outlet tubing were connected. The media outlet tubes fed into empty glass bottles as a way to determine whether even media outlet from each side of the tissue was achieved during the experiment. To remove any air bubbles in the chamber the media was purged into the chamber at an increased rate (25,000 $\mu L\ hr^{-1}$) for 45 seconds. After the initial purge, the media flow rate was reduced to 250 $\mu L\ hr^{-1}$ for the remainder of the experiment. The chambers, media, and full system box are all kept in an incubator set to 37 °C.

Live tissue experiments ranged from 24 h – 72 h, and a TEER measurement was performed every 2 hours. This created a timeline of the tissues TEER value to examine the TEER changes as a function of time. For each TEER measurement the input AC current magnitude was set at 85 μA and the frequency was swept from 12Hz to 5kHz at 20 different points. At each measurement point, the TEER was measured using the ohms law method as well. All the data was automatically saved to excel spreadsheets on the lab computer, and then processed by Python script.

After the experiment was completed, the chambers were disconnected from all tubing and disconnected from card edge connector. The chamber was then opened to expose the tissue sample and the tissue was preserved following the steps outlined in section *"Tissue Sectioning and Histochemistry"*.

Chapter 4 – Results and Discussions

4.1. System Electrical Performance

To characterize the impedance range, known resistances measured by an LCR meter with accuracy of 0.05% (GwInstek LCR-821) were compared to values calculated with this device (**Figure 4.1a**). The error threshold for the impedance calculation was set to 5%. With this threshold, the calculated impedance range is 150 – 6.5kΩ (**Figure 4.1b**). The limiting factor for the impedance range is the current and voltage gains of the read channel. The width of the impedance range (~6.485 kΩ) cannot be adjusted because the gain settings cannot be adjusted during the experiment. The impedance window (150 – 6.5kΩ) however, can be shifted up or down to fit the needed range for any different types of experiments.

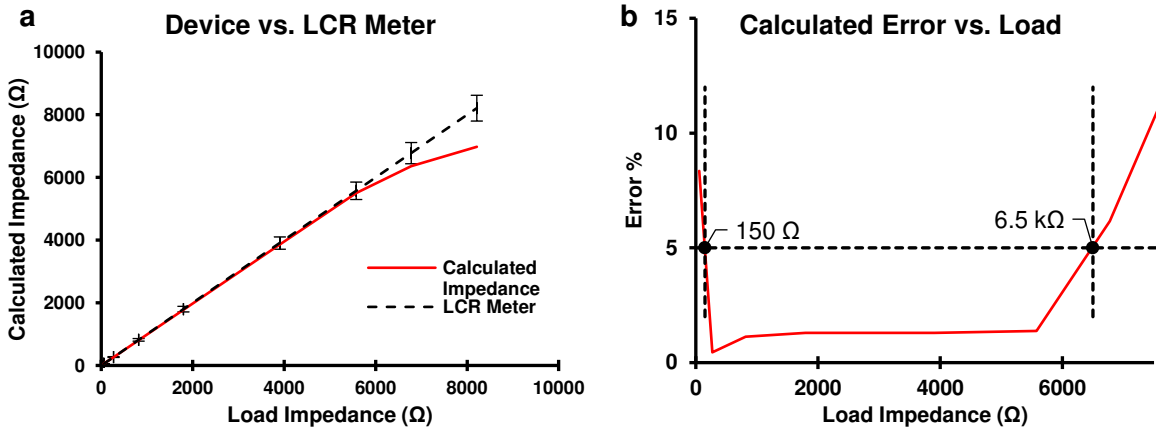

Figure 4.1: Impedance range and the calculated error. **a)** Calculated impedance vs. known impedance from LCR meter. **b)** Error as a function of load impedance, to find the true impedance range with <5% error.

The frequency response of each circuit component along the signal path is shown in **Figure 4.2a-d**. The component with the lowest bandwidth of 47.5 kHz is the TIA (**Figure 4.2d**). The bandwidth of the TIA was set by a compensation capacitor to be roughly ten times higher than the highest frequency of input sinusoidal stimulus (5kHz). This to not attenuate any important read channel signals while also filtering out as much high frequency noise as possible. It should be noted that the TIA tends to have high input inferred noise due to the high thermal noise of its gain-setting resistors. It also sits relatively late in the analog signal chain and its low bandwidth can filter out the output noise from other components (input level shifter and HCS) before it in the signal chain. This sets the full systems bandwidth at 47.5 kHz as intended.

The stability of each read channel is examined by its step response to obtain sufficiently damped responses (**Figure 4.2f**). The noise power spectral density (PSD) of the read channel was measured and shown in **Figure 4.2e**. The results show the total noise power to be 0.126 μV^2, well below the minimum output signal power of 82.1 μV^2 of the system, resulting in a signal-to-noise ratio (SNR) of 28.14 dB. Other system performance parameters, such as power consumption, TEER measurement error, and the acceptable TEER range with error less than 5%, were also measured and calculated. **Table 4.1** summarizes the system level electrical performance of the microphysiological system.

Table 4.1: Full System Specifications

Specification	**Value**	**Unit**
Impedance Calculation		
Frequency Range	10-5k	Hz
Impedance Range (Error <5%)	150-6.5k	Ω
Sampling		
ADC Sampling Rate	806.4k	samples/s
Resolution	12	bits
Power Consumption		
V_{dd}	±5	V
Full system	4.203	W
TEER Circuit Add on	1.17	W
Signal Processing		
Bandwidth	47.5	kHz
Howland Offset Current (DC)	1.87	μA
Voltage Gain	9.8214	gain
Current Gain	27,000	gain
Noise		
SNR	28.14	dB
Total Noise Power	0.1261	μV^2
Avg. Spectral Density	623.824	$nV/\sqrt{Hz}$
Spot Noise @ 100Hz	1685.79	$nV/\sqrt{Hz}$
Spot Noise @ 1kHz	630.688	$nV/\sqrt{Hz}$
Spot Noise @ 10kHz	762.691	$nV/\sqrt{Hz}$

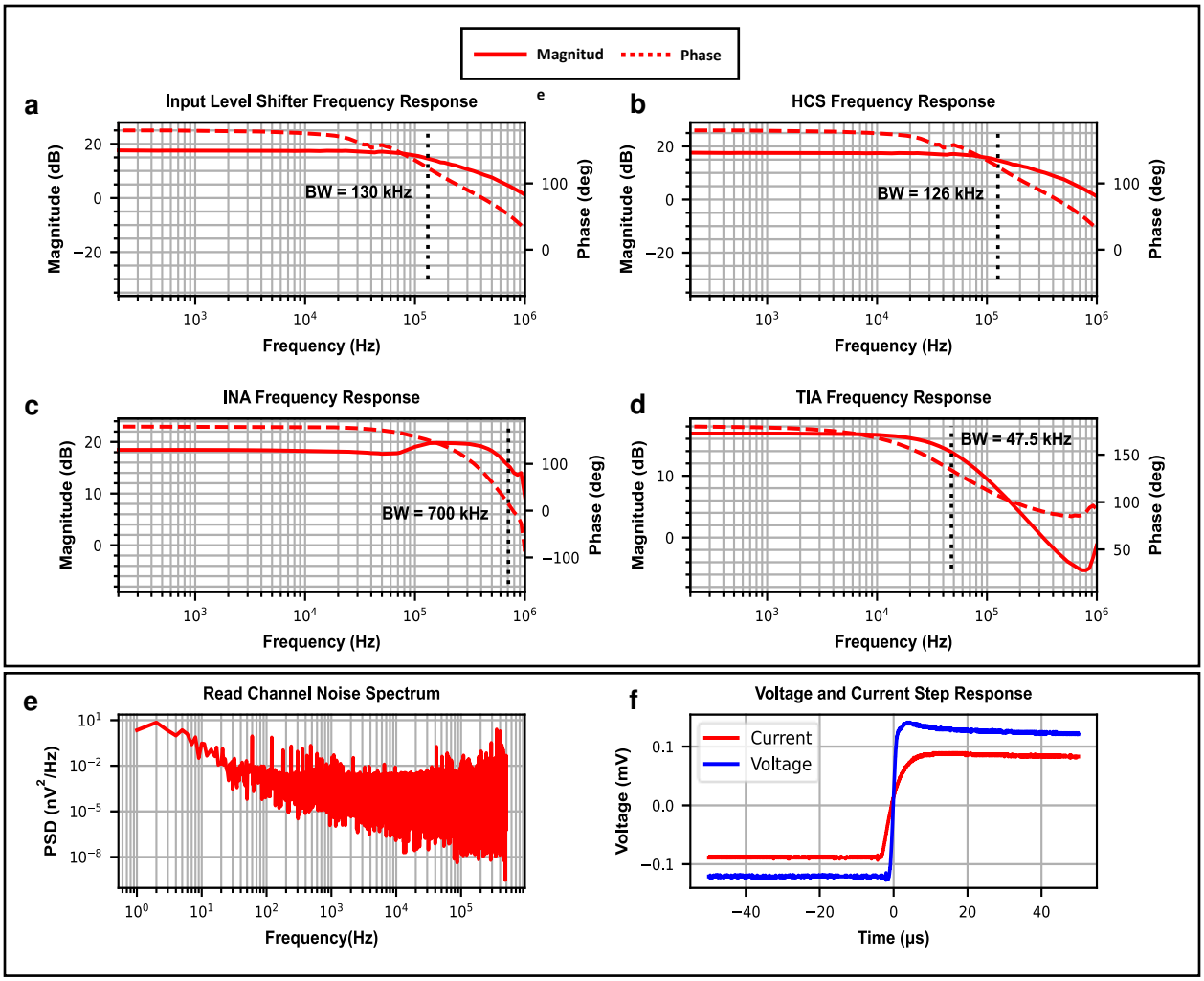

Figure 4.2: System electrical performance. The frequency response for each component in the signal path **(a-d)** was used to find the systems bandwidth. **a)** Input level shifter frequency response. **b)** HCS frequency response. **c)** INA frequency response. **d)** TIA frequency response. The limiting component is the TIA **(d)**, this component sets the systems bandwidth at 47.5kHz. **e)** The read channel noise power spectral density (PSD) was found to classify the noise specification of the system. **f)** The step response of the voltage (blue) and current (red) stages in the read channel. The lack of ringing in both step responses confirm the stability of the read channel.

4.2. Tissue Viability

Tissue health was maintained in the device with barrier integrity over 72 h. Colon explants maintained proper arrangement of mucosal, submucosal, muscular layers, and patterned crypts (**Figure 4.3a**(i)). To protect the body from potential pathogens, healthy intestinal tissue must maintain sophisticated epithelial and mucosal barriers. Specialized epithelial cells, known as goblet cells, are crucial to barrier maintenance as they are responsible for producing and secreting mucin. Goblet cells were characterized due to their essential roles in maintenance of the barrier. Goblet cell mucopolysaccharides were identified by binding *Ulex europaeus* agglutinin I (UEA-1) conjugated to rhodamine. After 72 h in the microphysiological system, goblet cells retained their distinct shape (**Figure 4.3a**(ii), arrows) and the inner

mucus layer remained intact confirming maintenance of the mucosal barrier (**Figure 4.3a**(ii)). To further verify barrier integrity, tight junctions were examined. Tight junctions adhere epithelial cells together forming a physical barrier between cells to prevent unwanted passage of ions and molecules between epithelial cells. Claudins are a specific type of tight junction protein that help form the backbone of tight junctions. Claudin-1 is widely expressed in the intestinal epithelium and has essential roles in tight junction integrity. After 72 h in the device, clear claudin-1 immunoreactivity remained around epithelial cells (**Figure 4.3a**(iii)) further indicating maintenance of tissue health and barrier integrity.

4.3. Using TEER to Measure Changes in Barrier Permeability

Changes in TEER were correlated with physiological signs of barrier impairment, such as alterations to epithelial cells, the mucus layer, and tight junction proteins. To induce a disruption to barrier permeability, the luminal side of colon tissue was treated with collagenase or acidic media. Bacterial collagenases are enzymes secreted by endogenous bacteria in the intestines that degrade collagen. Increased collagenase can break down tight junctions between epithelial cells, as well as, break down the extracellular matrix of epithelial cells [43]. This leads to increased intestinal permeability, and provides a model for the development of leaky gut syndrome [44]. We have previously shown that bacterial collagenase in luminal media can be used as a model to create leaky gut by disrupting epithelial cell (goblet cell) morphology and decreasing tight junction (claudin-1) expression [26]. Increased barrier permeability was shown by an increased reduction in TEER with collagenase treatment over time (**Figure 4.3b**(v)). To confirm that reductions in TEER correlated with physiological characteristics of increased intestinal permeability, goblet cells and claudin-1 were examined. Following collagenase treatment, goblet cells became more circular in shape (**Figure 4.3b**(i)) and claudin-1 immunoreactivity was moderately decreased (**Figure 4.3b**(iii)) indicating barrier impairment. To test whether changes in TEER matched changes in physiological changes, acidic media (pH 2) was added to the luminal side of tissue to induce significant damage to the intestinal barrier. Cells need to maintain a pH of 7.4 to function properly. Lowering the pH to 2.0 leads to significant epithelial cell death and alterations in cellular processes creating drastic increases in permeability. This was confirmed with goblet cells losing distinct shape and sloughing off near the lumen (**Figure 4.3b**(ii)). Claudin-1 immunoreactivity dramatically decreased indicating substantial loss of tight junctions (**Figure 4.3b**(iv)). These dramatic changes in epithelial cell and claudin-1 morphology correlate with the significant reduction of TEER following acidic pH treatment (**Figure 4.3b**(v))

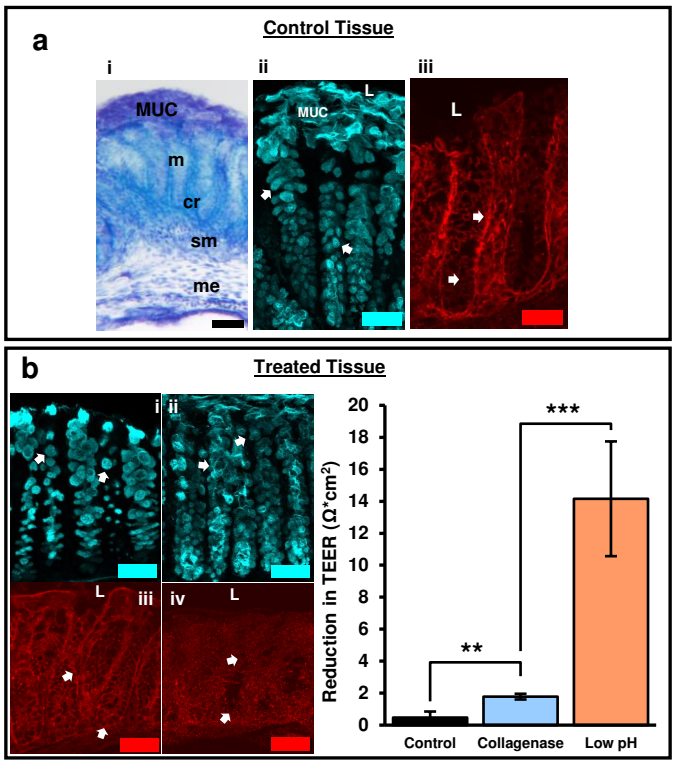

Figure 4.3: Tissue health was maintained over 72 h in the device and monitored after media treatment. **a)** Control tissue after 72 h experiment. i) Tol blue staining showing maintenance of colon morphology. ii) UEA-1^{+} material confirming maintenance of epithelial cells and mucus layer. iii) Claudin-1 immunoreactivity shows maintenance of tight junctions between epithelial cells and crypts indicated by claudin-1 immunoreactivity. MUC = mucus layer, m = mucosa, cr = crypt, sm = submucosa, me = muscularis externa, scale bars are 50µm for B and C, (need to figure out scale bars on bright field microscope). **b)** Collagenase treated, and acidic luminal media resulted in alterations in goblet cell morphology and tight junction expression indicative of increased barrier permeability. i) Goblet cells labeled with UEA-1 become circular after collagenase treatment. ii) Acidic media resulted in loss of goblet cell shape and sloughing off of cells near the lumen. iii) Alterations in tight junction protein expression (claudin-1) following collagenase treatment. iv) Claudin-1 expression decreased considerably with exposure to acidic media indicative of substantial barrier disruption. The bar graph shows a distinct reduction in TEER after exposure to different media composition. The difference in TEER was measured from 24 to 48-hour mark after the tissue was enclosed in the device, with the media change occurring at 24 hours. The three media compositions consist of a control media, collagenase treated media, and low pH media (more details about media composition in *"Animals, Tissue Collection, and Media Preparation"*). L = lumen, scale bars = 50µm, TEER values are normalized to the membrane surface area of the chamber, 0.0314cm^2. Control: n = 4, Collagenase: n = 10, Low pH: n = 3, **: $P < 0.005$; ***: $P < 0.0001$

4.4. Differences in Tissue Explant Detected by TEER

4.4.1. Cut Muscle vs. Intact Muscle

To determine whether distinct tissue components contributed differentially to TEER, the muscle layer was dissected away. Thereby removing the muscularis externa, a major subepithelial structure of the colon. TEER was measured after 24 h inside the chamber, allowing sufficient time for the tissue to equilibrate to its new environment. Removal of the muscle layer decreased TEER by about 39% (**Figure 4.4a**). This result is consistent with previous reports that have performed experiments to study the contribution of sub epithelial resistance. The values reported have ranged

from 15% to 80% of the total epithelial resistance is concentrated in the sub epithelium, depending on the location in the intestine as well as the animal [4], [37], [45]–[47]. Research using rat jejunum has shown a much larger contribution to total resistance done by the sub epithelium (78-80%)[4], [45]. Whereas measurements on the ileum, colon, and rectum in both rat and mice have showed much lower contributions (15-45%)[37], [46], [47]. This is consistent with the results found here using mouse colon.

Confirmation of total muscle dissection was done by Toluidine blue staining, as seen in **Figure 4.4a**(ii) when compared to tissue with the muscle intact (**Figure 4.4a**(i)). Demonstrating the TEER calculated with the muscle dissected is an accurate representation of the epithelial resistance alone and has little to no contribution from subepithelial resistances. This demonstration is lacking from all previous research studying the contribution of subepithelial resistance by subepithelial stripping or dissection[45]–[47]. These images alongside the TEER measurements provide new evidence for the contribution of subepithelial resistance to total epithelial resistance.

4.4.2. Proximal vs. Distal Colon

Since distal colon is generally thicker than proximal colon, we investigated if these differences in tissue thickness correlated with changes in TEER. Based on the results that an intact muscle layer increased TEER (**Figure 4.4a**), we expected TEER to be higher in distal colon. However, we observed about a 19% decrease in TEER in the distal colon compared to the proximal colon (**Figure 4.4b**). Interestingly, this is consistent with previous reports showing higher TEER values in mouse proximal colon compared to mid or distal colon[6]. Based on the observed effect of muscle removal, we found it likely that other factors contribute to differences in TEER between proximal and distal colon. One possible factor is luminal pH. The pH of the proximal colon is typically around 5.8-6.5, while the distal colon is typically around 7-7.6[48]. Previous studies have attributed increased TEER to decreased pH in the culture media[49] and this is consistent with our observations that an empty chamber filled with acidic media (pH 2) had higher TEER than control media (pH 7.4).

Higher TEER in proximal colon may be a function of the thickness of the mucus layer. The colon houses the majority of the intestinal microbiome and, therefore, has a thick mucus layer that physically separates bacteria from underlying epithelial cells. The proximal colon has been reported to have a thicker mucus layer compared to the distal colon with increased number and size of goblet cells, as well as increased expression of mucin-2[50]. In vivo measurements of mouse colon have estimated the colon mucus layer to be ~190 μm[51]. This is significant as the total tissue thickness

of mouse colon is estimated to be is around 140-300 µm[52]. The mucus layer may have a profound effect on TEER, however, studies investigating the contribution of the mucus layer on TEER are lacking. The mucus layer can be easily

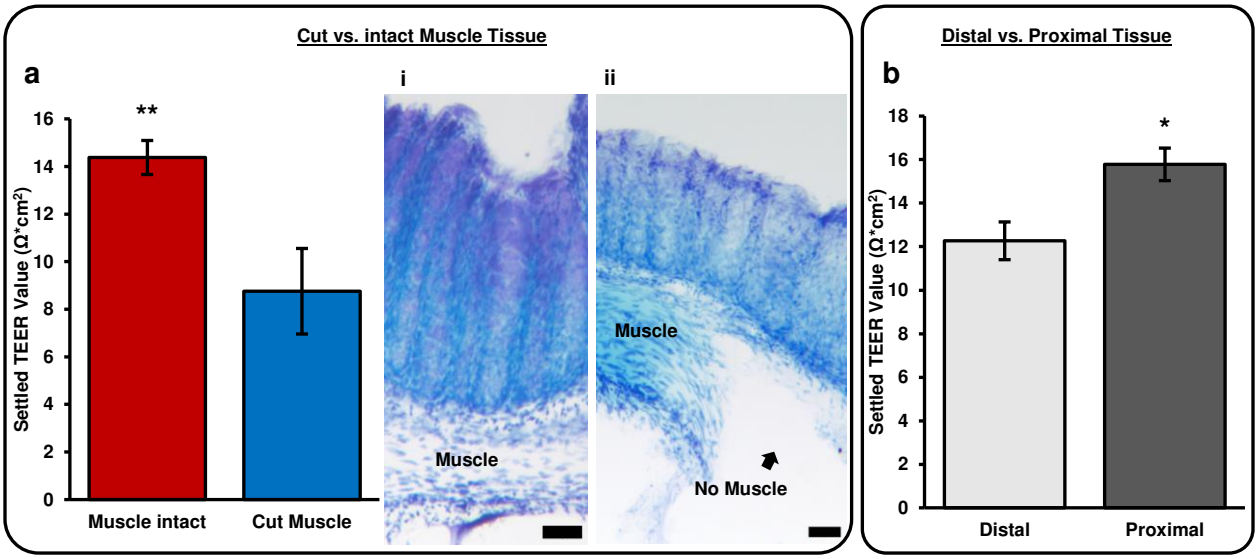

Figure 4.4: Physical differences in tissue explant. **a)** This bar chart shows the difference in settled TEER value of tissues explants with the muscle intact vs. with the muscle removed. The settled TEER value is taken 24 hours after the tissue is enclosed in the chamber. i) Tol blue staining of tissue with intact muscle. ii) Tol blue staining tissue with muscle removed. **b)** Settled TEER values for different regions of mouse colon tissue. Proximal tissue was defined as the three pieces of tissue closest to the cecum and distal tissue was defined as the two pieces farthest from the cecum and closest to the rectum. Each tissue piece was approximately 5mm in length. The settled TEER value was taken approximately 24 hours after the tissue had been enclosed in the device. Muscle intact: n = 15, Cut muscle: n = 7, Distal: n = 6, Proximal: n = 9, **: $P < 0.005$, *: $P < 0.01$.

washed off in tissue dissection and preparation.

4.5. Highlights of System Performance

Besides the electrical performance metrics and the experimental results shown above, some unique capabilities of the microphysiological system are compared with the existing systems/devices reported in the literature as illustrated in **Table 4.2**. Compared to the existing systems/devices, this system is able to maintain longer tissue viability of intestine tissue with integrated electrodes to provide real-time TEER measurements. The custom electronics and system design also provide experiment configuration and improved throughput.

Table 4.2: Comparison of epithelial barrier investigation devices

	Biological Sample		Electrical Permeability				Chamber/System Design	
	Sample Type	**Tissue Viability**	**TEER capable?**	**Electrode Type**	**Stimulus Signal**	**Measurement Electronics**	**Microfluidics Support**	**# Devices**
Transwell [8], [9]	Cell monolayer	-	Yes	Ag/AgCl "stick" electrodes	DC	Commercial Benchtop	No	96
Liang et al., 2023[16]	Cell monolayer (canine kidney)	-	Yes	Integrated glass chip	Up to 10MHz	Commercial Benchtop	Yes	1
Helm et al., 2019[20]	Cell monolayer (Caco-2)	-	Yes	Polycarbonate substrate electrode chips	Up to 100kHz	Commercial Benchtop	Yes	1
Fernandes et al., 2022[38]	Cell monolayer (GI tract and airway)	-	Yes	Integrated glass chip	Up to 100kHz	Custom-built	One side only	8
Navicyte[6]	Mouse and human intestinal tissue	<3 h	Yes	Ag/AgCl "stick" electrodes	DC	Commercial Benchtop	No	6
Clarke et al., 2009[2]	Mouse colon tissue	3 h	Yes	Ag/AgCl electrodes connected by salt bridge	DC	Commercial Benchtop	No	1
Calvo et al., 2020[3]	Frog epithelial tissue	-	Yes	Integrated "stick" electrodes	Up to 100kHz	Custom-built	No	1
Dawson et al., 2016[25]	Human intestine tissue	72 h	No	-	-	-	Yes	1
Poenar et al., 2020[31]	Porcine esophageal tissue	48	Yes	Integrated "stick" electrodes	DC	Commercial Benchtop	Yes	1
Cherwin et al., 2023[26] **& Richardson et al., 2020**[27]	Mouse colon tissue	72 h	No	-	-	-	Yes	1
Amirabadi et al., 2022[53]	Porcine & human colon tissue	24 h	No	Optical Fiber Sensor	-	-	Yes	1
This Work	Mouse colon tissue	72 h	Yes	Integrated glass chip	Up to 5kHz	Custom-built	Yes	3

Chapter 5 – Conclusion and Future Work

5.1. Conclusion

This thesis presents a highly integrated microphysiological system for studying live tissue barrier permeability of mouse colon. The unique design of the microfluidic chamber is capable of securing an explant of mouse colon tissue between two independent media pathways creating a microenvironment inside the chamber comparable to the environment in vivo. The use of proper media provides nutrients, support gut microbiome, and create important oxygen gradients across the tissue to keep tissue viability for an extended period of time. After 72 hours in the chamber, the tissue explants displayed an inner mucus layer, robust goblet cells, and evident tight junction function along the length of the epithelial layer. These characteristics all serve as strong indicators of sustained barrier integrity. This preservation of tissue viability addresses a significant drawback in existing live tissue barrier permeability devices.

Integrated electrode chips allow the microfluidic chamber to successfully characterize barrier permeability using TEER measurements in real time. The plug-and-play nature of the system design simplifies the experiment setup and allows for all chambers to be re-usable and universal. Unlike most existing systems where bulky and expensive benchtop equipment is needed to perform experiments, the integrated support electronics made the overall system small enough to fit into an incubator. Furthermore, architectural scalability allows multiple chambers to be connected to the system enabling higher throughput of controlled experiments using samples from the same donor. The use of the system is further enhanced by a custom-built GUI which was developed to allow each experiment to be customizable and ran from any host computer.

In conclusion, this microphysiological system has the potential to open new avenues to investigate barrier health of live tissues. Real time barrier health measurements are crucial to developing more accurate ex vivo tissue models for studying the health and chemical response of epithelial cells.

5.2. Future work

5.2.1. Four-point measurement

To avoid intrinsic error on the on the impedance measurement, the voltage and current electrodes should be set up using a four-point electrode setup. A two-point setup introduces unwanted lead resistance from the electrodes to the sample impedance. Using a four-point setup the voltage electrodes read the voltage directly across the sample, separate

from the current electrodes. This avoids any potential drop from the current lead resistance. The current design only allows for a three-point setup. In this design the positive input of the INA is directly connected to the input voltage electrode, and the negative input of the INA is directly connected to the common mode voltage (0V). Ideally, the INA will be connected to a voltage electrode on each side of the biological sample. The current design ran into problems for two reasons. First, the output electrode is connected to the virtual ground of the TIA. This adds noise to the negative input of the INA. Second, the common mode rejection ratio of the INA may be insufficient for the amount of noise generated on the electrodes.

5.2.2. HCS output impedance

The output impedance of the HCS is crucial to providing a constant current stimulus to the electrodes. The current design employed low tolerance (<0.1%) resistors. This achieved a high enough output impedance to prove the functionality of the HCS, however, to better improve the current reading, the output impedance should be improved. To achieve better resistor matching, resistor trimming can be employed. By placing a trimming potentiometer in series with the input 150 kΩ resistor (**Figure 3.9a**), will allow for better matching on the positive feedback resistors.

5.2.3. ADC Sampling Frequency

The most limiting aspect of the current design is the limited ADC sampling frequency. The ADC sampling frequency limits the input frequency that can be sampled without any error. We found that the current sampling rate (806.4 ksps) can sample an input up to 5kHz before exceeding the error threshold. To fully characterize the biological samples impedance spectrum, the stimulus frequency should ideally be able to reach 1MHz. The reason for the limited sampling rate of this design is due to the master clock from the FTDI microcontroller. The maximum SPI clock using the FTDI is 30MHz, this will need to be greatly increased to achieve a greater sampling rate. There are several ways that this could be achieved. The first way this could be achieved is by replacing the FTDI with a different high-speed ARM microcontroller, this could potentially increase the SPI clock frequency tenfold. The downside to this option is that the entire system would have to be configured to the new microcontroller. It would also mean that the software for the entire system would need to be updated and most likely rewritten. Another option could be to use an external high-speed clock. Using an external clock IC is most likely the cheapest solution and requires the smallest amount of change to the current design. To do this would require the ADC output to be directly deposited into a memory chip.

The memory can then be read at a slower rate by the FTDI at a later time. The difficult aspect of this solution will be timing the chip-select pins to synchronize with an external clock.

5.2.4. Phase Calculation

Along with the magnitude response, the phase response can be used to characterize different components in the biological samples equivalent circuit. The frequency response is not complete without both of these graphs. The current design is only capable of accurately calculating the magnitude plot, all the results found using this device are based on the magnitude alone. The device currently does not have an accurate enough method of calculating phase response from the voltage and current signals. To confirm the phase of the electrode setup in the chamber demonstrates the expected output, the phase response of the chamber when measured using an LCR meter (GwInstek LCR-821). In **Figure 5.1a**, the phase response of the LCR meter at four different time points throughout the experiment can be seen.

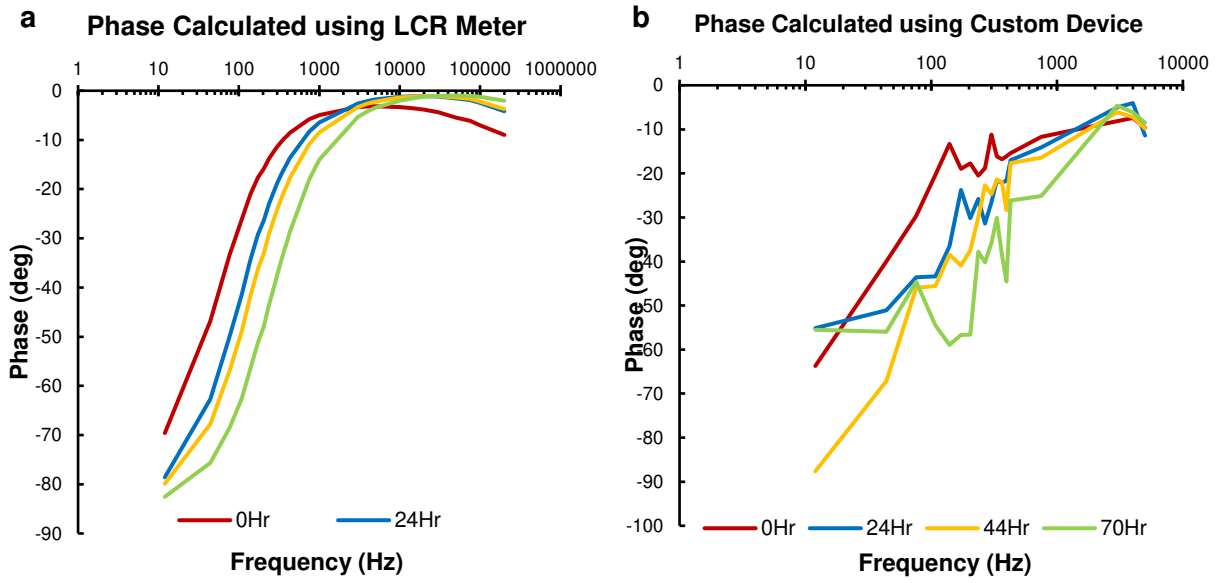

Figure 5.1: Phase calculation of tissue sample. a) Phase response at four different time points (0, 24, 45, and 70hr into the experiment) calculated using commercial LCR meter. b) Phase response of the same tissue sample at the same time points using the custom microphsyiological system.

Then in **Figure 5.1b**, the phase response of the same tissue at the same time points can be seen to be much less accurate however still roughly following the same trend. The LCR phase response (**Figure 5.1a)** shows what is expected with a reduction in resistance of the biological barrier, proving the chamber and electrodes are not the issue. The issue lies in the methodology behind the phase calculation. The problem is most likely due to the fact that the voltage and current samples are sampled individually, one after the other. This is because the microcontroller is only capable of reading one signal at a time. Reading the voltage and signal signals separately introduces a large amount of error to the timing

of the signal reading. In an attempt to solve this issue, a phase calculation circuit was developed but was not used in the final system. Continuing work on this circuit could be a method of solving the phase calculation issue. Another solution for this issue, a memory chip at the output of the ADC could be used to save the data of the voltage and current simultaneously, then read to the FTDI one at a time later.

5.2.5. Phase Calculation Circuit

A phase calculation circuit was designed to calculate phase of the biological sample more accurately. The circuit was tested and showed promise, however never made it out of the testing phase, where it could be used in the final system design. The circuit is a completely custom design where the voltage and current sinusoids are converted to square waves using high slew rate op-amps, the rising edge time difference is equal to the sinusoidal peak time difference. The square waves are then fed into an XOR gate creating a pulse with the width representing the peak time difference between sinusoidal signals. The pulse width of the circuit needs to be converted to an analog signal before being level shifted and inputted into the ADC. To do this, the pulse goes through an integrator to create saw tooth type signal, where the slope of the climb is determined by R_{int} and C_{int}. This saw tooth signal can then be sampled by the ADC without issue and sent to the computer where the phase can be calculated. If the slope of the sawtooth wave is known, then finding the height of the climb represents the time difference between sinusoidal peaks. This circuit allows the

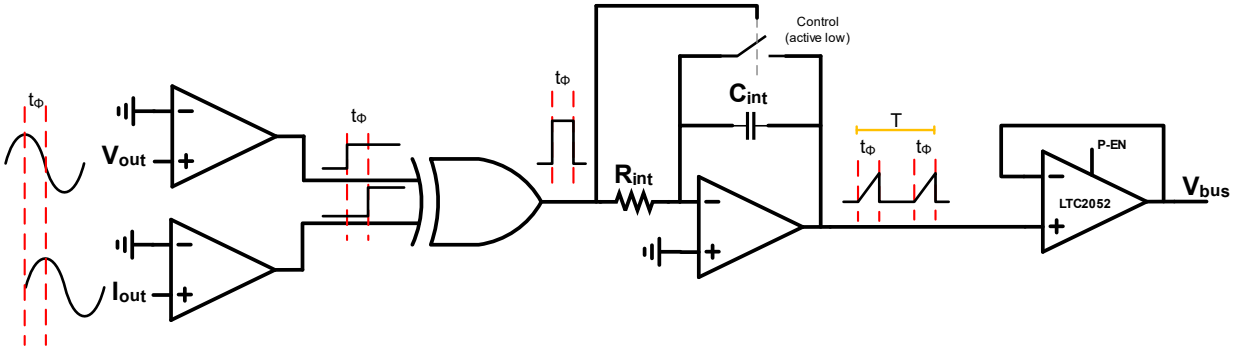

Figure 5.2: Phase calculation circuit concept

phase difference to be calculated from a single signal as opposed to comparing the voltage and current outputs. The concept of the phase calculation circuit can be seen in **Figure 5.2**.

This circuit still requires hardware and software debugging. Every component in the circuit adds error to the generated time difference signal. This means that to have an accurate phase measurement, all op-amps and digital components must be fast enough to not add substantial delay. Another issue is the DC shift on the output voltage, if the voltage signal is entirely below the reference voltage (0V) then no square wave is generated after the first stage. However

initial tests show that if at least one full period of the voltage square wave is generated, then the different height saw tooths can be averaged together to find the true phase difference. The final step to implementing this circuit is writing an algorithm that can take the sampled saw tooth signal and calculate the phase difference.

5.2.6. Added Gain Options

The impedance range of the device is limited by the current and voltage gain of the read channels. To increase this range there needs to be a way to change the gain settings in real time. The current design allows for one gain setting, this was based on the known impedance range needed for the experiment at hand. To change the current and voltage gain, the physical resistors on the board need to be changed out for a new value. To improve versatility of the device, there should be several gain settings available on the board. This allows the impedance range to adapt to the load impedance if it happens to be out of the original range.

5.2.7. GUI Customization Capability

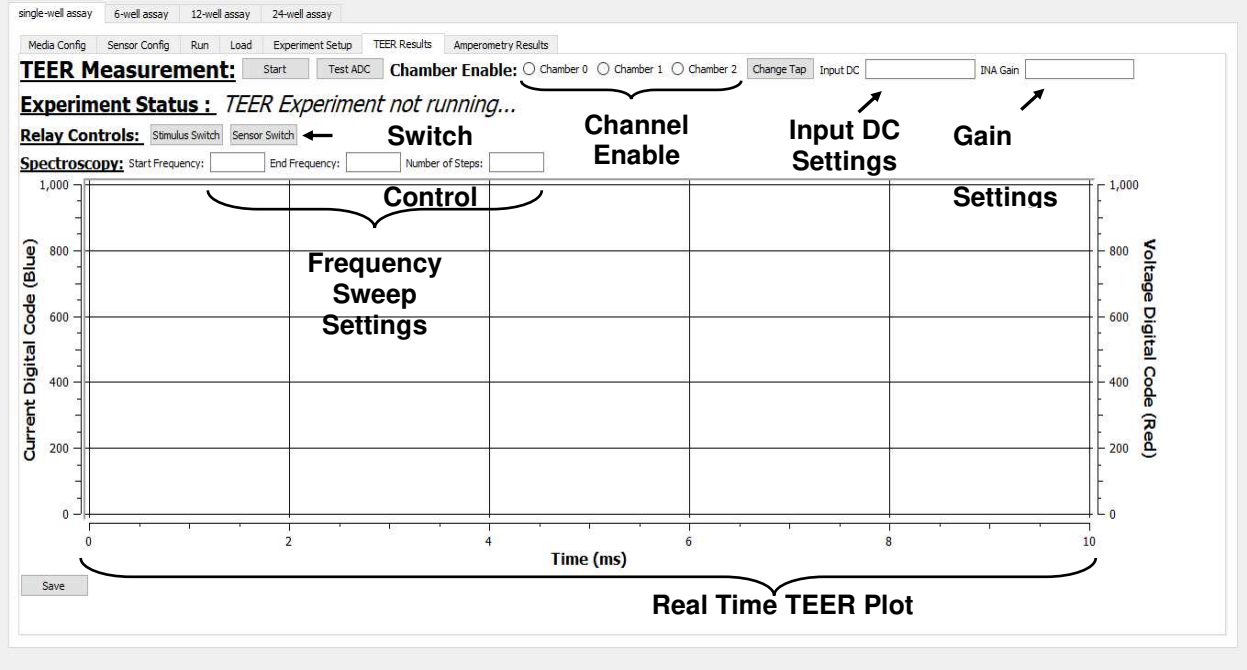

Figure 5.3: Potential GUI layout for experiment customization features

Custom GUI is capable of many different customization settings for an experiment. The current GUI has not implemented most of the features seen in **Figure 5.3**, because the software that performs the experiment operations was still being developed. In the end, the goal of this device is to have a user interface that is capable of controlling every aspect that would be needed by a researcher. An initial layout has been created, highlighting the different

capabilities the GUI can be used for. This is for future iterations of this project to be implemented. Some of the added features include, a real-time TEER plot, customizable frequency sweep settings, switch control, individual channel enables, input DC settings, gain settings, and more. Ideally, the experiment should be able to be controlled from this singular page.

References

[1] H. H. Ussing and K. Zerahn, "Active transport of sodium as the source of electric current in the short-circuited isolated frog skin," *Acta Physiol Scand*, vol. 23, no. 2–3, pp. 110–127, Aug. 1951, doi: 10.1111/j.1748-1716.1951.tb00800.x.

[2] L. L. Clarke, "A guide to Ussing chamber studies of mouse intestine," *American Journal of Physiology-Gastrointestinal and Liver Physiology*, vol. 296, no. 6, pp. G1151–G1166, Jun. 2009, doi: 10.1152/ajpgi.90649.2008.

[3] P. C. Calvo, O. Campo, C. Guerra, S. Castaño, and F. Fonthal, "Design of using chamber system based on electrical impedance spectroscopy (EIS) to measure epithelial tissue," *Sensing and Bio-Sensing Research*, vol. 29, p. 100357, Aug. 2020, doi: 10.1016/j.sbsr.2020.100357.

[4] M. Fromm, J. D. Schulzke, and U. Hegel, "Epithelial and subepithelial contributions to transmural electrical resistance of intact rat jejunum, in vitro," *Pflugers Arch*, vol. 405, no. 4, pp. 400–402, Dec. 1985, doi: 10.1007/BF00595695.

[5] S. A. Weiner *et al.*, "Rectal potential difference and the functional expression of CFTR in the gastrointestinal epithelia in cystic fibrosis mouse models," *Pediatr Res*, vol. 63, no. 1, pp. 73–78, Jan. 2008, doi: 10.1203/PDR.0b013e31815b4bc6.

[6] A. Thomson *et al.*, "The Ussing chamber system for measuring intestinal permeability in health and disease," *BMC Gastroenterol*, vol. 19, no. 1, p. 98, Jun. 2019, doi: 10.1186/s12876-019-1002-4.

[7] A. H. Gitter, J.-D. Schulzke, D. Sorgenfrei, and M. Fromm, "Ussing chamber for high-frequency transmural impedance analysis of epithelial tissues," *Journal of Biochemical and Biophysical Methods*, vol. 35, no. 2, pp. 81–88, Sep. 1997, doi: 10.1016/S0165-022X(97)00028-6.

[8] F. Leonard, E.-M. Collnot, and C.-M. Lehr, "A three-dimensional coculture of enterocytes, monocytes and dendritic cells to model inflamed intestinal mucosa in vitro," *Mol Pharm*, vol. 7, no. 6, pp. 2103–2119, Dec. 2010, doi: 10.1021/mp1000795.

[9] F. R. Walter *et al.*, "A versatile lab-on-a-chip tool for modeling biological barriers," *Sensors and Actuators B: Chemical*, vol. 222, pp. 1209–1219, Jan. 2016, doi: 10.1016/j.snb.2015.07.110.

[10] H. Nazari *et al.*, "Advances in TEER measurements of biological barriers in microphysiological systems," *Biosensors and Bioelectronics*, vol. 234, p. 115355, Aug. 2023, doi: 10.1016/j.bios.2023.115355.

[11] F. Ghiselli, B. Rossi, A. Piva, and E. Grilli, "Assessing Intestinal Health. In Vitro and Ex vivo Gut Barrier Models of Farm Animals: Benefits and Limitations," *Front Vet Sci*, vol. 8, p. 723387, 2021, doi: 10.3389/fvets.2021.723387.

[12] J. Wegener, D. Abrams, W. Willenbrink, H.-J. Galla, and A. Janshoff, "Automated multi-well device to measure transepithelial electrical resistances under physiological conditions," *Biotechniques*, vol. 37, no. 4, pp. 590, 592–594, 596–597, Oct. 2004, doi: 10.2144/04374ST03.

[13] J. Wegener, A. Hakvoort, and H.-J. Galla, "Barrier function of porcine choroid plexus epithelial cells is modulated by cAMP-dependent pathways in vitro," *Brain Research*, vol. 853, no. 1, pp. 115–124, Jan. 2000, doi: 10.1016/S0006-8993(99)02317-3.

[14] J. Yeste, X. Illa, M. Alvarez, and R. Villa, "Engineering and monitoring cellular barrier models," *J Biol Eng*, vol. 12, no. 1, p. 18, Dec. 2018, doi: 10.1186/s13036-018-0108-5.

[15] C. M. Leung *et al.*, "A guide to the organ-on-a-chip," *Nat Rev Methods Primers*, vol. 2, no. 1, Art. no. 1, May 2022, doi: 10.1038/s43586-022-00118-6.

[16] F. Liang *et al.*, "A microfluidic tool for real-time impedance monitoring of in vitro renal tubular epithelial cell barrier," *Sensors and Actuators B: Chemical*, vol. 392, p. 134077, Oct. 2023, doi: 10.1016/j.snb.2023.134077.

[17] L. Gijzen *et al.*, "An Intestine-on-a-Chip Model of Plug-and-Play Modularity to Study Inflammatory Processes," *SLAS Technol*, vol. 25, no. 6, pp. 585–597, Dec. 2020, doi: 10.1177/2472630320924999.

[18] M. W. van der Helm *et al.*, "Direct quantification of transendothelial electrical resistance in organs-on-chips," *Biosensors and Bioelectronics*, vol. 85, pp. 924–929, Nov. 2016, doi: 10.1016/j.bios.2016.06.014.

[19] R. Thuenauer, E. Rodriguez-Boulan, and W. Römer, "Microfluidic approaches for epithelial cell layer culture and characterisation," *Analyst*, vol. 139, no. 13, pp. 3206–3218, Jul. 2014, doi: 10.1039/c4an00056k.

[20] M. W. van der Helm *et al.*, "Non-invasive sensing of transepithelial barrier function and tissue differentiation in organs-on-chips using impedance spectroscopy," *Lab Chip*, vol. 19, no. 3, pp. 452–463, Jan. 2019, doi: 10.1039/C8LC00129D.

[21] B. Srinivasan, A. R. Kolli, M. B. Esch, H. E. Abaci, M. L. Shuler, and J. J. Hickman, "TEER Measurement Techniques for In Vitro Barrier Model Systems," *SLAS Technology*, vol. 20, no. 2, pp. 107–126, Apr. 2015, doi: 10.1177/2211068214561025.
[22] I. C. McLean, L. A. Schwerdtfeger, S. A. Tobet, and C. S. Henry, "Powering *ex vivo* tissue models in microfluidic systems," *Lab Chip*, vol. 18, no. 10, pp. 1399–1410, 2018, doi: 10.1039/C8LC00241J.
[23] M. Astolfi *et al.*, "Micro-dissected tumor tissues on chip: an ex vivo method for drug testing and personalized therapy," *Lab Chip*, vol. 16, no. 2, pp. 312–325, 2016, doi: 10.1039/C5LC01108F.
[24] S. Yasotharan, S. Pinto, J. G. Sled, S.-S. Bolz, and A. Günther, "Artery-on-a-chip platform for automated, multimodal assessment of cerebral blood vessel structure and function," *Lab Chip*, vol. 15, no. 12, pp. 2660–2669, 2015, doi: 10.1039/C5LC00021A.
[25] A. Dawson *et al.*, "A microfluidic chip based model for the study of full thickness human intestinal tissue using dual flow," *Biomicrofluidics*, vol. 10, no. 6, p. 064101, Nov. 2016, doi: 10.1063/1.4964813.
[26] A. E. Cherwin, H. N. Templeton, A. T. Ehrlich, B. H. Patlin, C. S. Henry, and S. A. Tobet, "Microfluidic organotypic device to test intestinal mucosal barrier permeability *ex vivo*," *Lab Chip*, p. 10.1039.D3LC00615H, 2023, doi: 10.1039/D3LC00615H.
[27] A. Richardson, L. A. Schwerdtfeger, D. Eaton, I. Mclean, C. S. Henry, and S. A. Tobet, "A microfluidic organotypic device for culture of mammalian intestines *ex vivo*," *Anal. Methods*, vol. 12, no. 3, pp. 297–303, 2020, doi: 10.1039/C9AY02038A.
[28] N. Yissachar *et al.*, "An Intestinal Organ Culture System Uncovers a Role for the Nervous System in Microbe-Immune Crosstalk," *Cell*, vol. 168, no. 6, pp. 1135-1148.e12, Mar. 2017, doi: 10.1016/j.cell.2017.02.009.
[29] E. Moens and M. Veldhoen, "Epithelial barrier biology: good fences make good neighbours," *Immunology*, vol. 135, no. 1, pp. 1–8, Jan. 2012, doi: 10.1111/j.1365-2567.2011.03506.x.
[30] S. Siri, Y. Zhao, F. Maier, D. M. Pierce, and B. Feng, "The Macro- and Micro-Mechanics of the Colon and Rectum I: Experimental Evidence," *Bioengineering (Basel)*, vol. 7, no. 4, p. 130, Oct. 2020, doi: 10.3390/bioengineering7040130.
[31] D. P. Poenar, G. Yang, W. K. Wan, and S. Feng, "Low-Cost Method and Biochip for Measuring the Trans-Epithelial Electrical Resistance (TEER) of Esophageal Epithelium," *Materials (Basel)*, vol. 13, no. 10, p. 2354, May 2020, doi: 10.3390/ma13102354.
[32] M. Knowles, J. Gatzy, and R. Boucher, "Increased bioelectric potential difference across respiratory epithelia in cystic fibrosis," *N Engl J Med*, vol. 305, no. 25, pp. 1489–1495, Dec. 1981, doi: 10.1056/NEJM198112173052502.
[33] O. A. Itani *et al.*, "Human cystic fibrosis airway epithelia have reduced Cl- conductance but not increased Na+ conductance," *Proc Natl Acad Sci U S A*, vol. 108, no. 25, pp. 10260–10265, Jun. 2011, doi: 10.1073/pnas.1106695108.
[34] J. R. Riordan *et al.*, "Identification of the cystic fibrosis gene: cloning and characterization of complementary DNA," *Science*, vol. 245, no. 4922, pp. 1066–1073, Sep. 1989, doi: 10.1126/science.2475911.
[35] K. Benson, S. Cramer, and H.-J. Galla, "Impedance-based cell monitoring: barrier properties and beyond," *Fluids and Barriers of the CNS*, vol. 10, no. 1, p. 5, Jan. 2013, doi: 10.1186/2045-8118-10-5.
[36] N. J. Douville, Y.-C. Tung, R. Li, J. D. Wang, M. E. H. El-Sayed, and S. Takayama, "Fabrication of two-layered channel system with embedded electrodes to measure resistance across epithelial and endothelial barriers," *Anal Chem*, vol. 82, no. 6, pp. 2505–2511, Mar. 2010, doi: 10.1021/ac9029345.
[37] A. H. Gitter, M. Fromm, and J.-D. Schulzke, "Impedance analysis for the determination of epithelial and subepithelial resistance in intestinal tissues," *Journal of Biochemical and Biophysical Methods*, vol. 37, no. 1–2, pp. 35–46, Sep. 1998, doi: 10.1016/S0165-022X(98)00016-5.
[38] J. Fernandes *et al.*, "Real-time monitoring of epithelial barrier function by impedance spectroscopy in a microfluidic platform," *Lab Chip*, vol. 22, no. 10, pp. 2041–2054, May 2022, doi: 10.1039/D1LC01046H.
[39] J. Liu, X. Qiao, M. Wang, W. Zhang, G. Li, and L. Lin, "The differential Howland current source with high signal to noise ratio for bioimpedance measurement system," *Rev Sci Instrum*, vol. 85, no. 5, p. 055111, May 2014, doi: 10.1063/1.4878255.
[40] "AN-1515 A Comprehensive Study of the Howland Current Pump," Texas Intsruments, Application Report SNOA474A.
[41] N. Nguyen *et al.*, "Microfluidic models of the human circulatory system: versatile platforms for exploring mechanobiology and disease modeling," *Biophys Rev*, vol. 13, no. 5, pp. 769–786, Oct. 2021, doi: 10.1007/s12551-021-00815-8.
[42] Y. M. Obeidat, M.-H. Cheng, G. Catandi, E. Carnevale, A. J. Chicco, and T. W. Chen, "Design of a multi-sensor platform for integrating extracellular acidification rate with multi-metabolite flux measurement for small

biological samples," *Biosensors and Bioelectronics*, vol. 133, pp. 39–47, May 2019, doi: 10.1016/j.bios.2019.02.069.
[43] A. S. Duarte, A. Correia, and A. C. Esteves, "Bacterial collagenases - A review," *Crit Rev Microbiol*, vol. 42, no. 1, pp. 106–126, 2016, doi: 10.3109/1040841X.2014.904270.
[44] R. S. Aleman, M. Moncada, and K. J. Aryana, "Leaky Gut and the Ingredients That Help Treat It: A Review," *Molecules*, vol. 28, no. 2, p. 619, Jan. 2023, doi: 10.3390/molecules28020619.
[45] M. Hemlin, M. Jodal, O. Lundgren, H. Sjövall, and L. Stage, "The importance of the subepithelial resistance for the electrical properties of the rat jejunum *in vitro*," *Acta Physiologica Scandinavica*, vol. 134, no. 1, pp. 79–88, Sep. 1988, doi: 10.1111/j.1748-1716.1988.tb08462.x.
[46] Y.-H. Tai and C.-Y. Tai, "The conventional short-circuiting technique under-short-circuits most epithelia," *J. Membrain Biol.*, vol. 59, no. 3, pp. 173–177, Oct. 1981, doi: 10.1007/BF01875423.
[47] A. H. Gitter, K. Bendfeldt, J. D. Schulzke, and M. Fromm, "Trans/paracellular, surface/crypt, and epithelial/subepithelial resistances of mammalian colonic epithelia," *Pflugers Arch - Eur J Physiol*, vol. 439, no. 4, pp. 477–482, Feb. 2000, doi: 10.1007/s004249900202.
[48] A. E. Mikolajczyk, S. Watson, B. L. Surma, and D. T. Rubin, "Assessment of Tandem Measurements of pH and Total Gut Transit Time in Healthy Volunteers," *Clinical and Translational Gastroenterology*, vol. 6, no. 7, p. e100, Jul. 2015, doi: 10.1038/ctg.2015.22.
[49] H. C. Helms, H. S. Waagepetersen, C. U. Nielsen, and B. Brodin, "Paracellular tightness and claudin-5 expression is increased in the BCEC/astrocyte blood-brain barrier model by increasing media buffer capacity during growth," *AAPS J*, vol. 12, no. 4, pp. 759–770, Dec. 2010, doi: 10.1208/s12248-010-9237-6.
[50] K. Bergstrom *et al.*, "Proximal colon–derived O-glycosylated mucus encapsulates and modulates the microbiota," *Science*, vol. 370, no. 6515, pp. 467–472, Oct. 2020, doi: 10.1126/science.aay7367.
[51] F. Hugenholtz and W. M. De Vos, "Mouse models for human intestinal microbiota research: a critical evaluation," *Cell. Mol. Life Sci.*, vol. 75, no. 1, pp. 149–160, Jan. 2018, doi: 10.1007/s00018-017-2693-8.
[52] M. A. Abdelrahman *et al.*, "High-Frequency Ultrasound for In Vivo Measurement of Colon Wall Thickness in Mice," *Ultrasound in Medicine & Biology*, vol. 38, no. 3, pp. 432–442, Mar. 2012, doi: 10.1016/j.ultrasmedbio.2011.12.011.
[53] H. Eslami Amirabadi *et al.*, "Intestinal explant barrier chip: long-term intestinal absorption screening in a novel microphysiological system using tissue explants," *Lab Chip*, vol. 22, no. 2, pp. 326–342, 2022, doi: 10.1039/D1LC00669J.

Appendix A – TEER Calculation Board Schematic

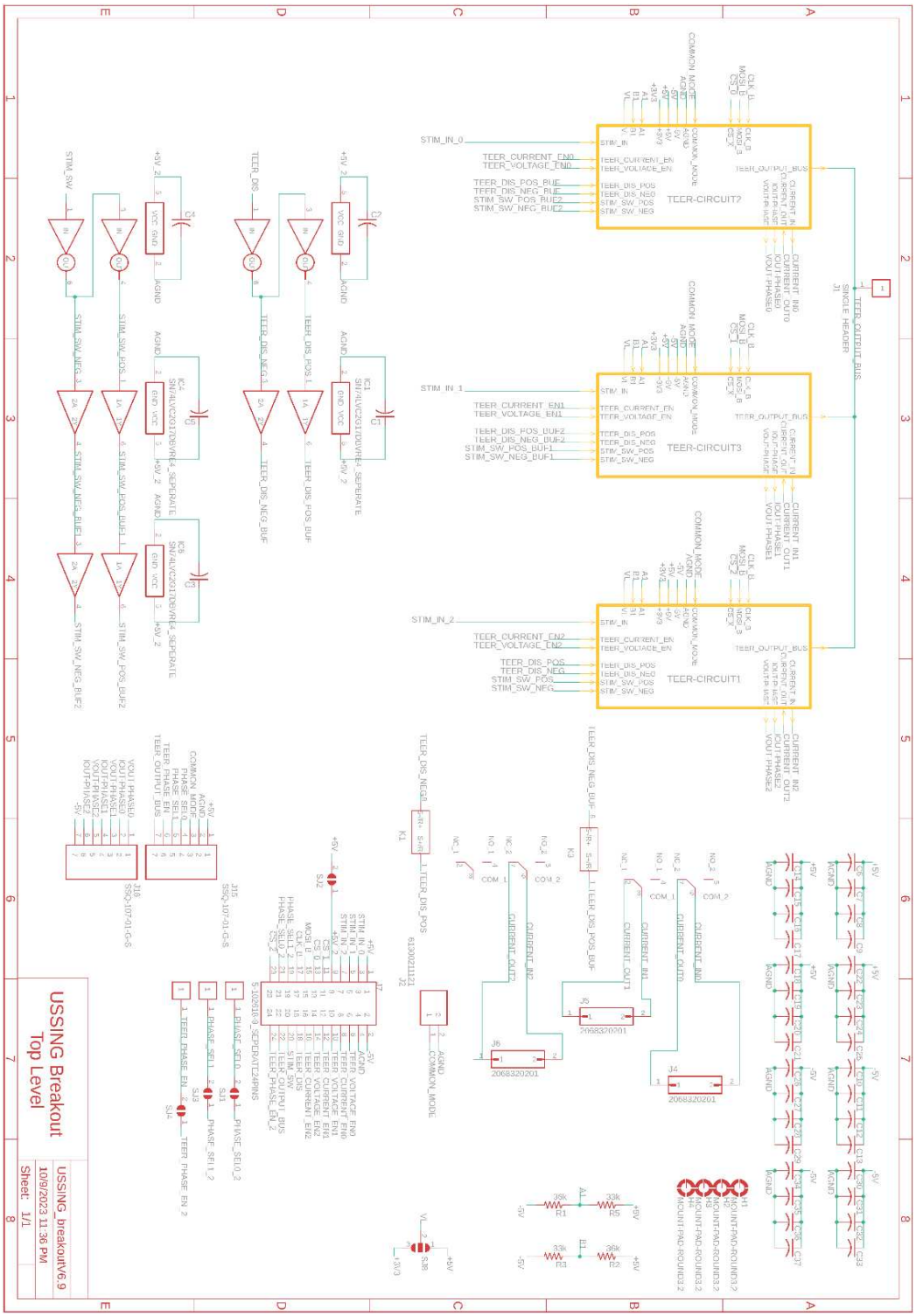

Figure A - 1: Top level circuit in PCB design software (EAGLE) of the TEER calculation board. This level contains each chambers individual TEER circuit, headers to connector to the main board, extra bypass capacitors, and more.

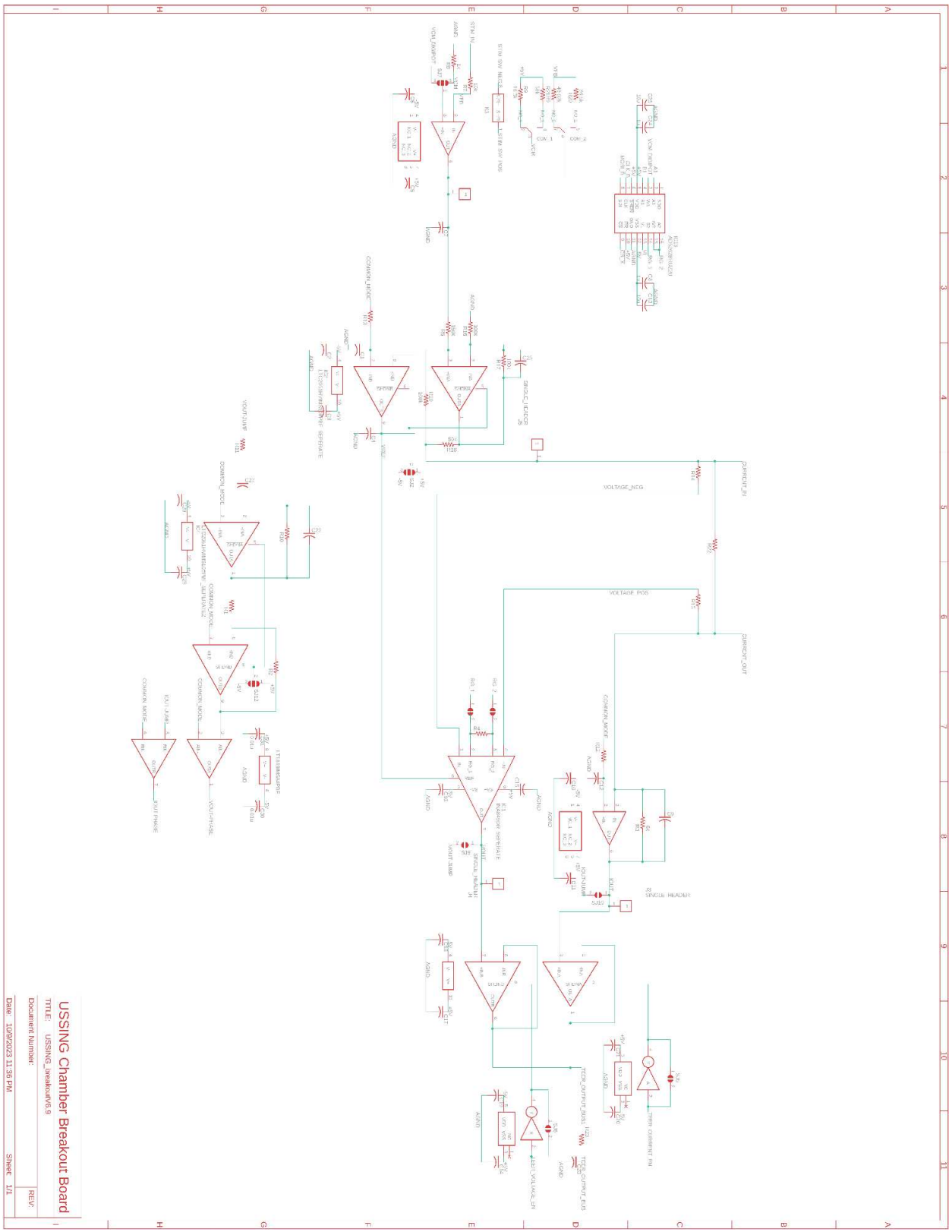

Figure A - 2: Final TEER calculation circuit for the PCB. This module is reused three times, one for each chamber, in the top-level circuit for the TEER calculation board.

Appendix B – Main Control Board Schematic

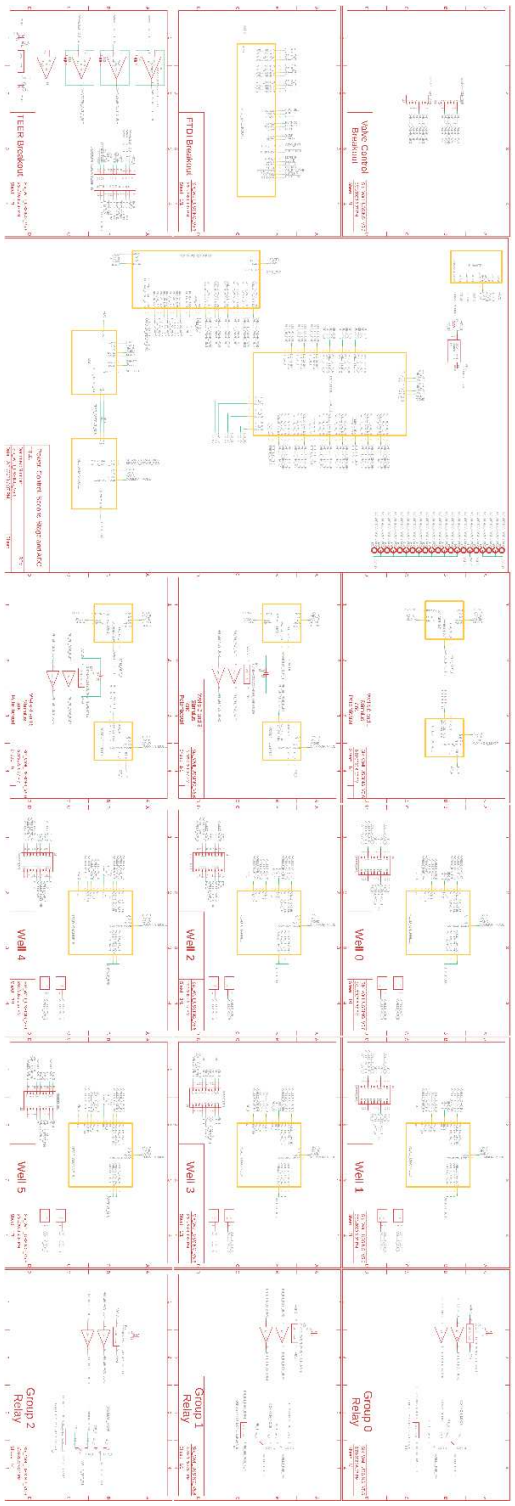

Figure B - 1: Top level PCB circuit for the main control board. This board provides the power supply, microcontroller, control signals, analog-to-digital converter, and more. This top-level circuit is designed to be hierarchical and made up of many module circuits seen below.

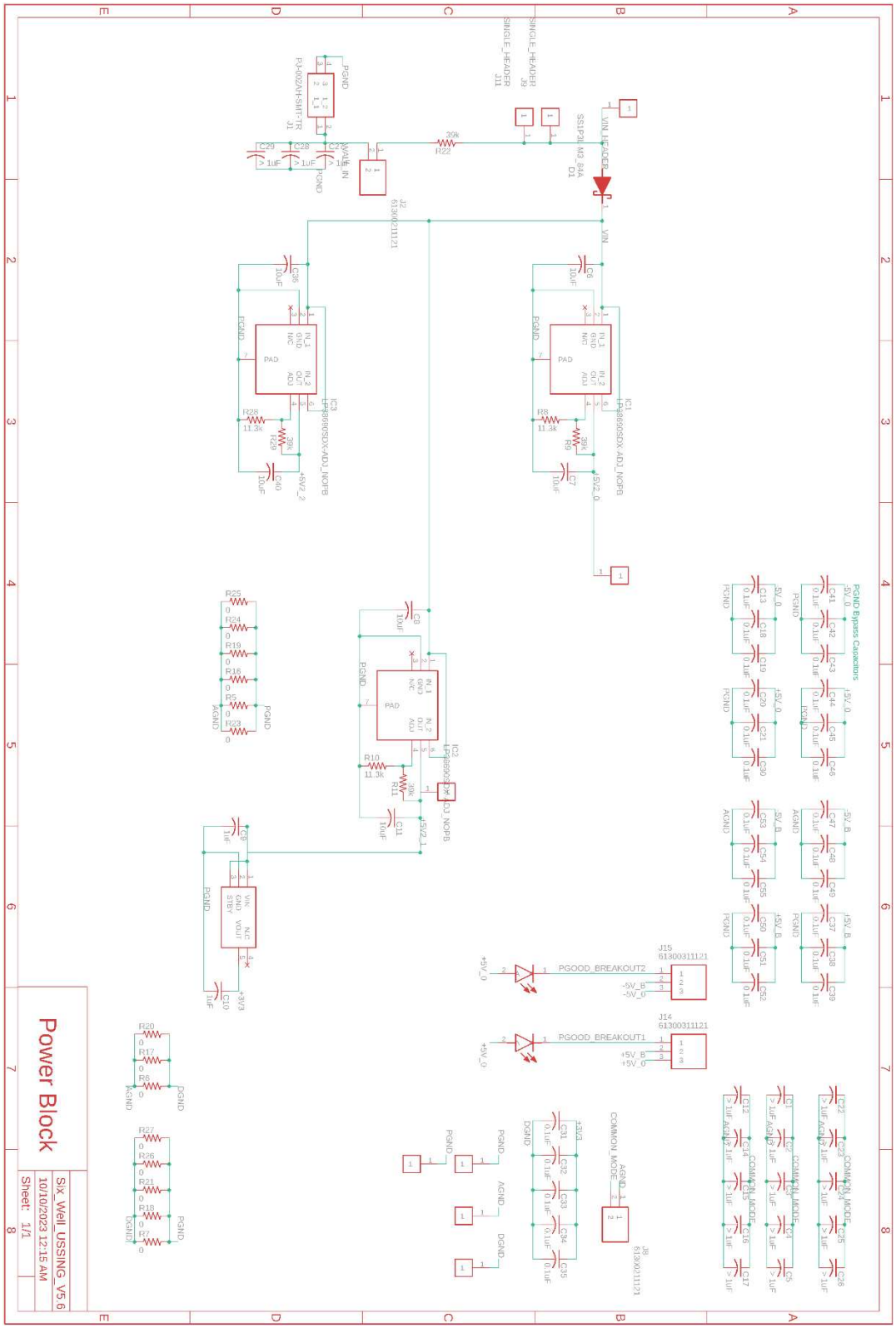

Figure B - 2: Power supply circuit that is housed on the main control board. This circuit includes three 5.5V LDO's that provide power to the external +/- 5V power supply boards. This circuit also includes the 3.3V LDO that provides power to all the digital electronics.

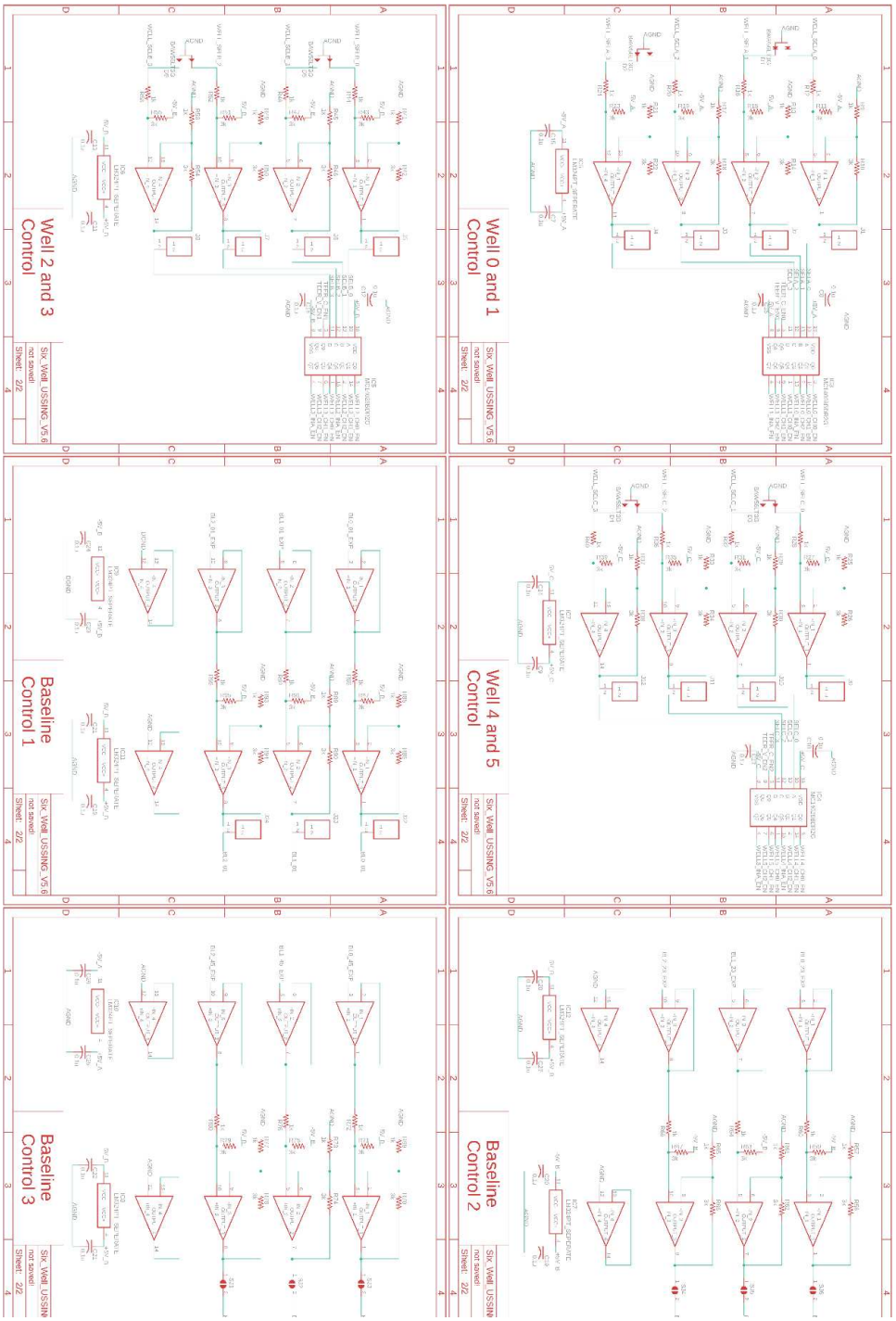

Figure B - 3: Control signal level shifters. Used to make the control signals from the microcontroller the appropriate voltage levels.

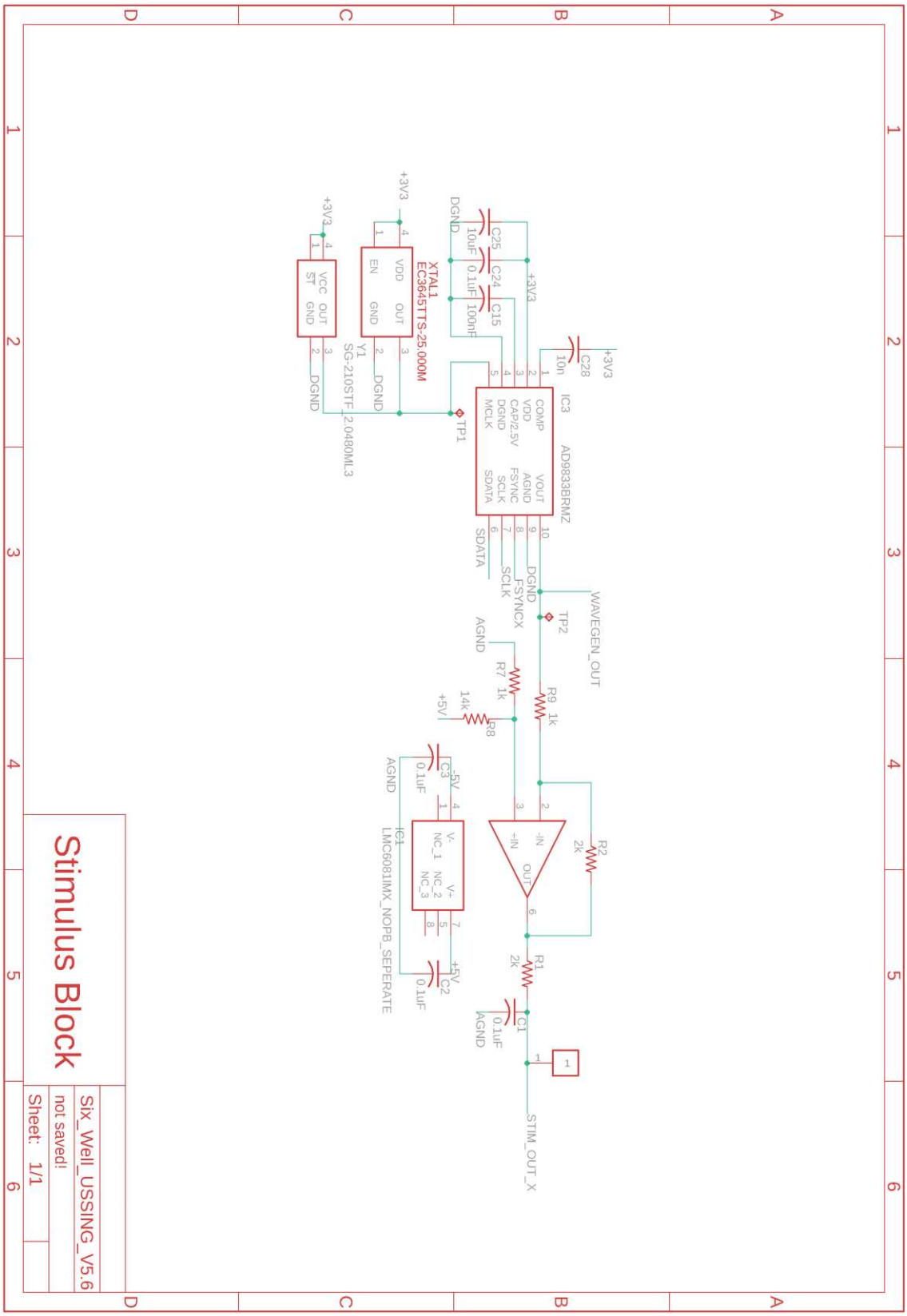

Figure B - 4: Signal generator circuit. Contains the programmable wave-gen chip, AD9833, that provides the stimulus signals for all experiments performed with this device.

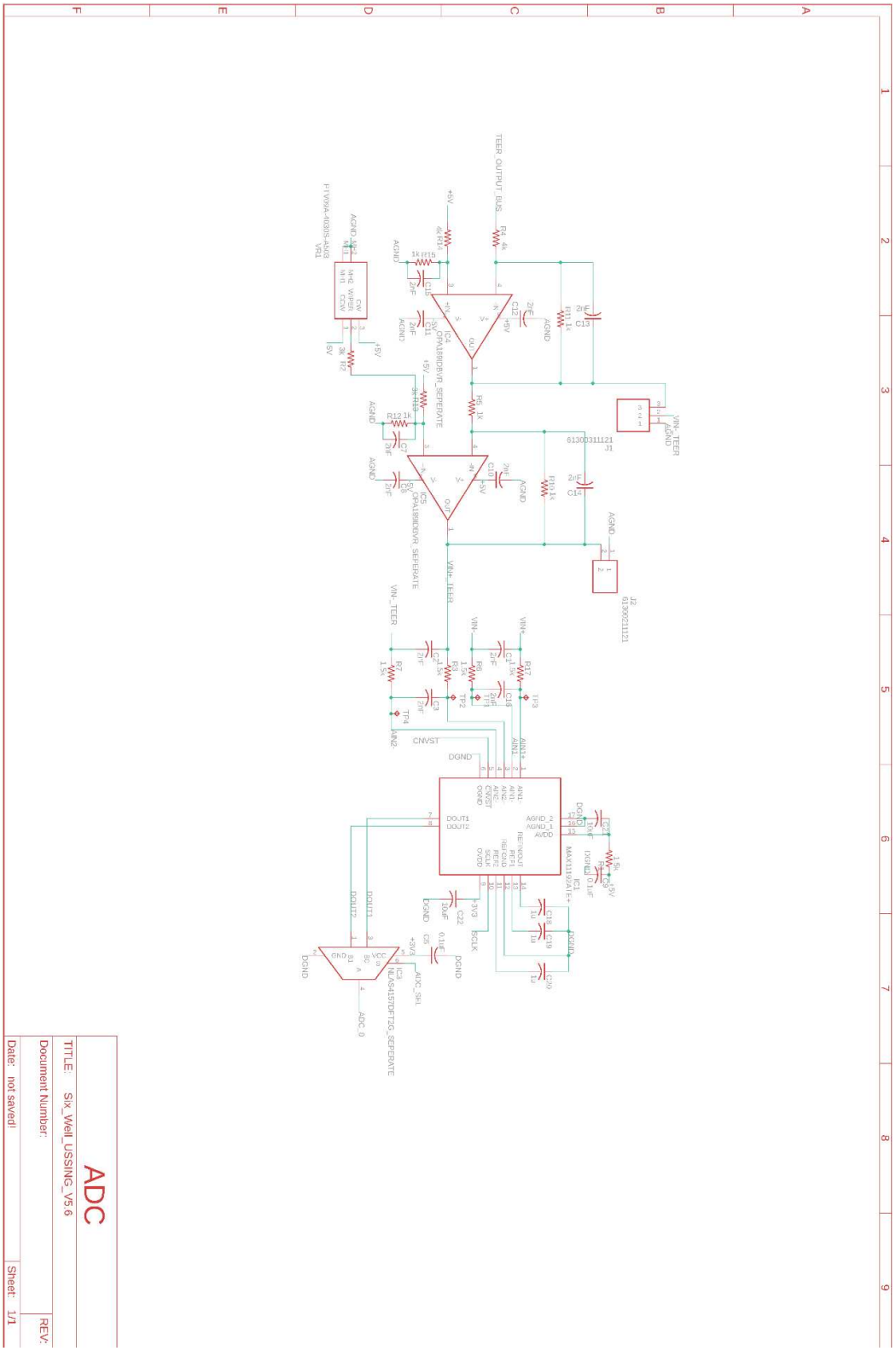

Figure B - 5: Analog-to-digital converter (ADC) circuit. The ADC converts the output analog signal from the read channels to a digital value that is sent to the microcontroller and then the host computer. This block also contains circuitry to convert the single-ended analog signal to differential before going into the ADC.

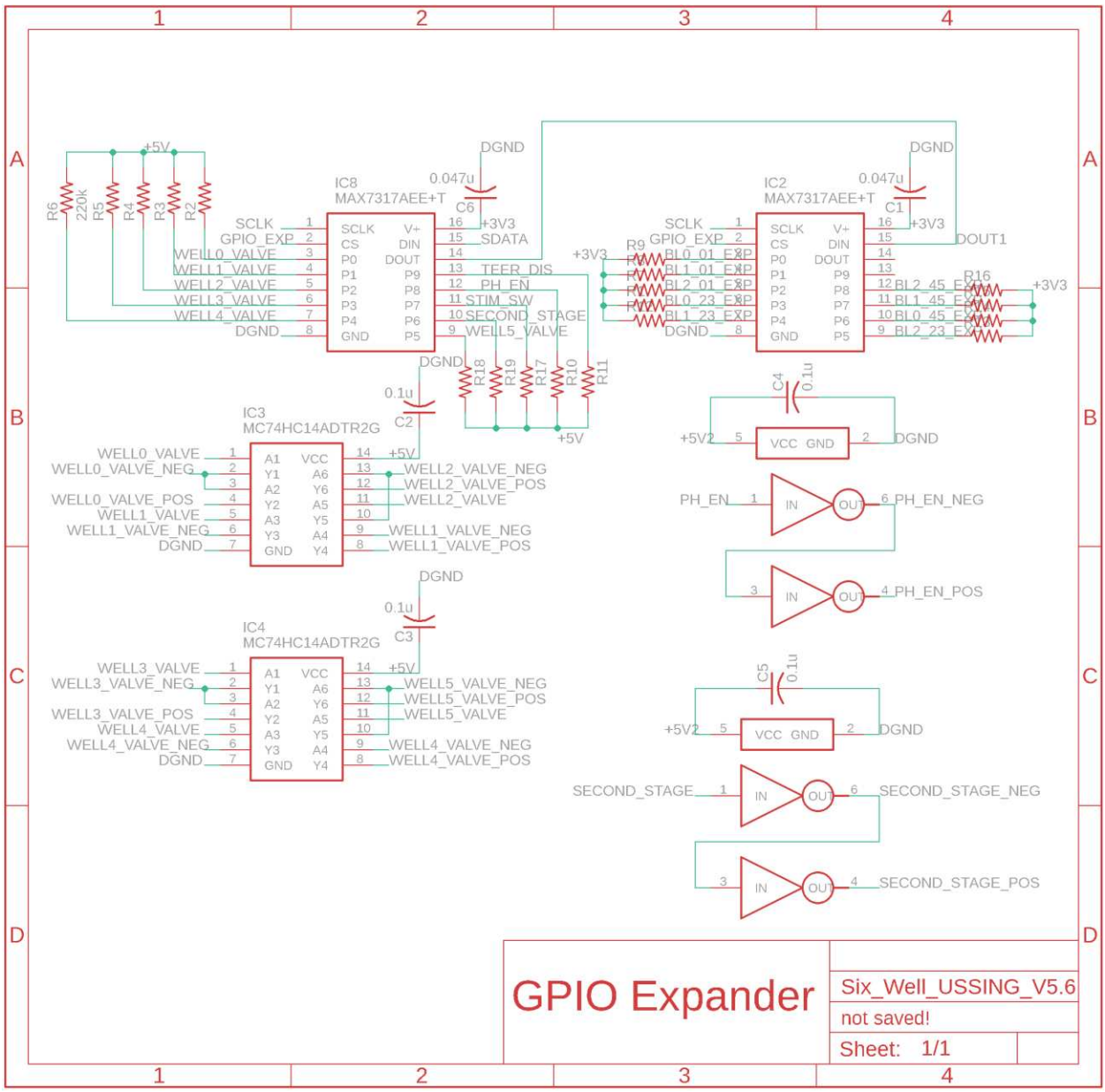

Figure B - 6: GPIO-expanders block. The GPIO-expanders provide additionally needed control signals for the system.

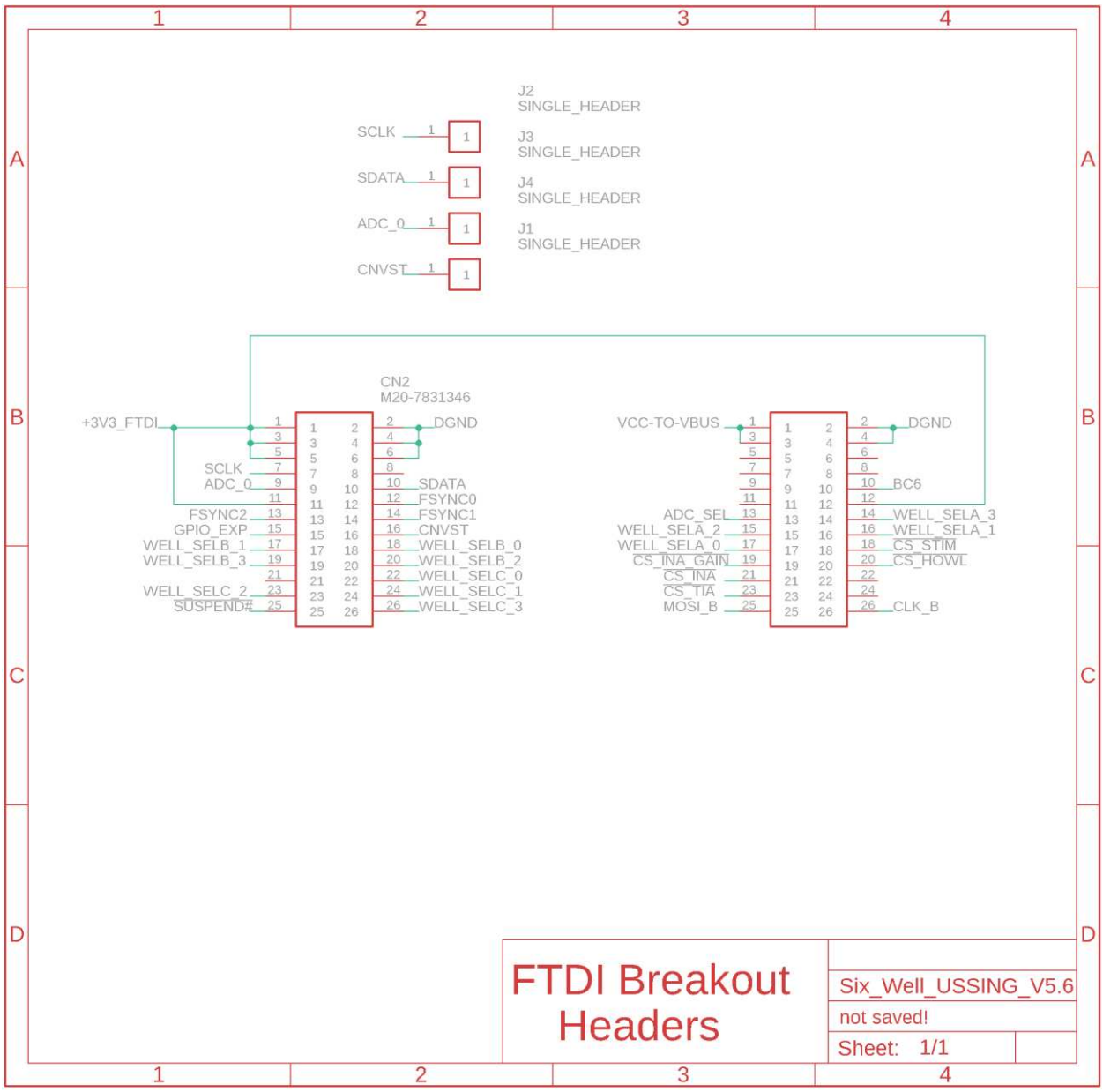

Figure B - 7: FTDI microcontroller headers that allow the FTDI breakout board to be directly plugged into the main control board.

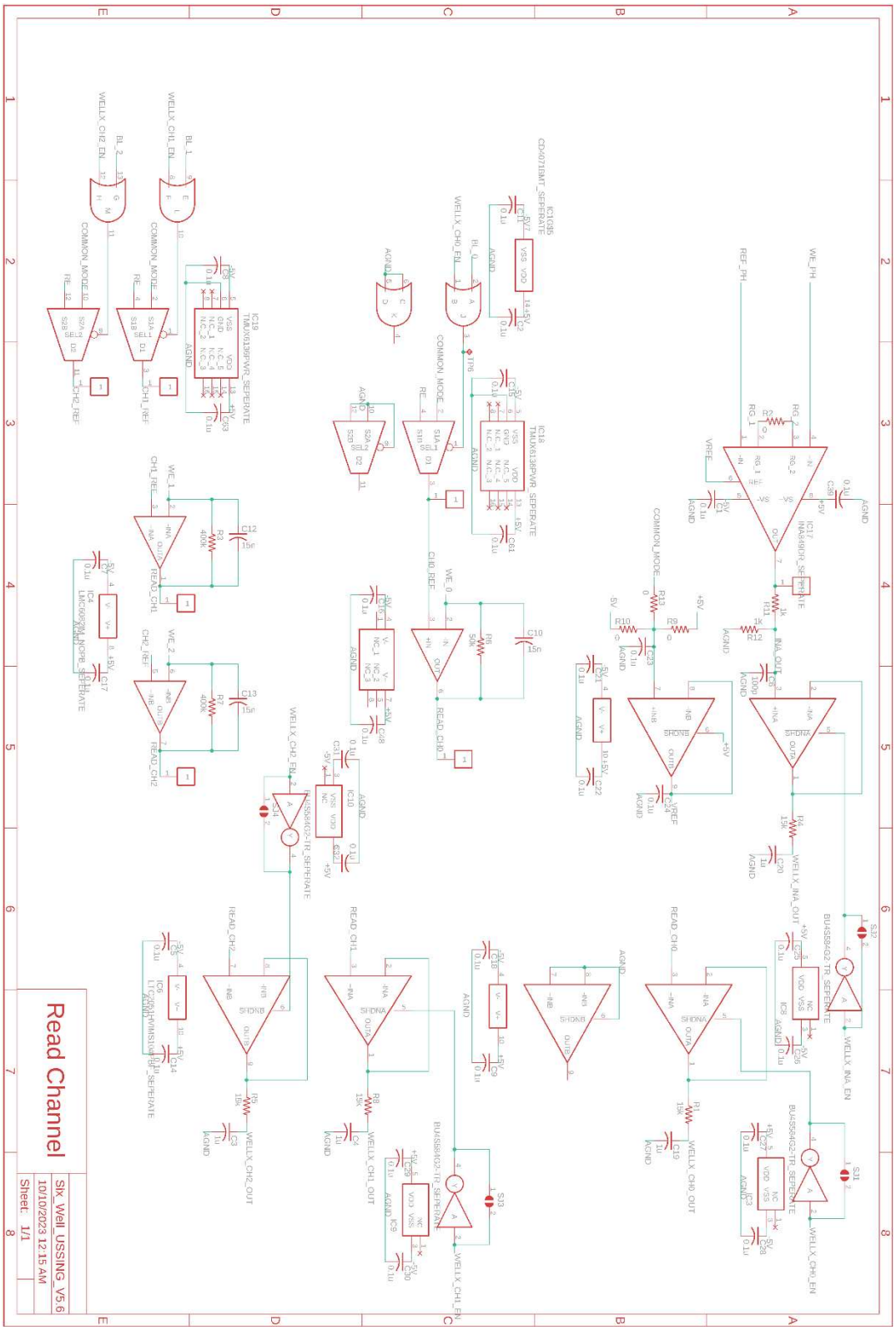

Figure B - 8: Metabolic measurements read channel circuitry. This read channel is used for various other metabolic measurements that are not included in this thesis.

Appendix C – Phase Calculation Schematic

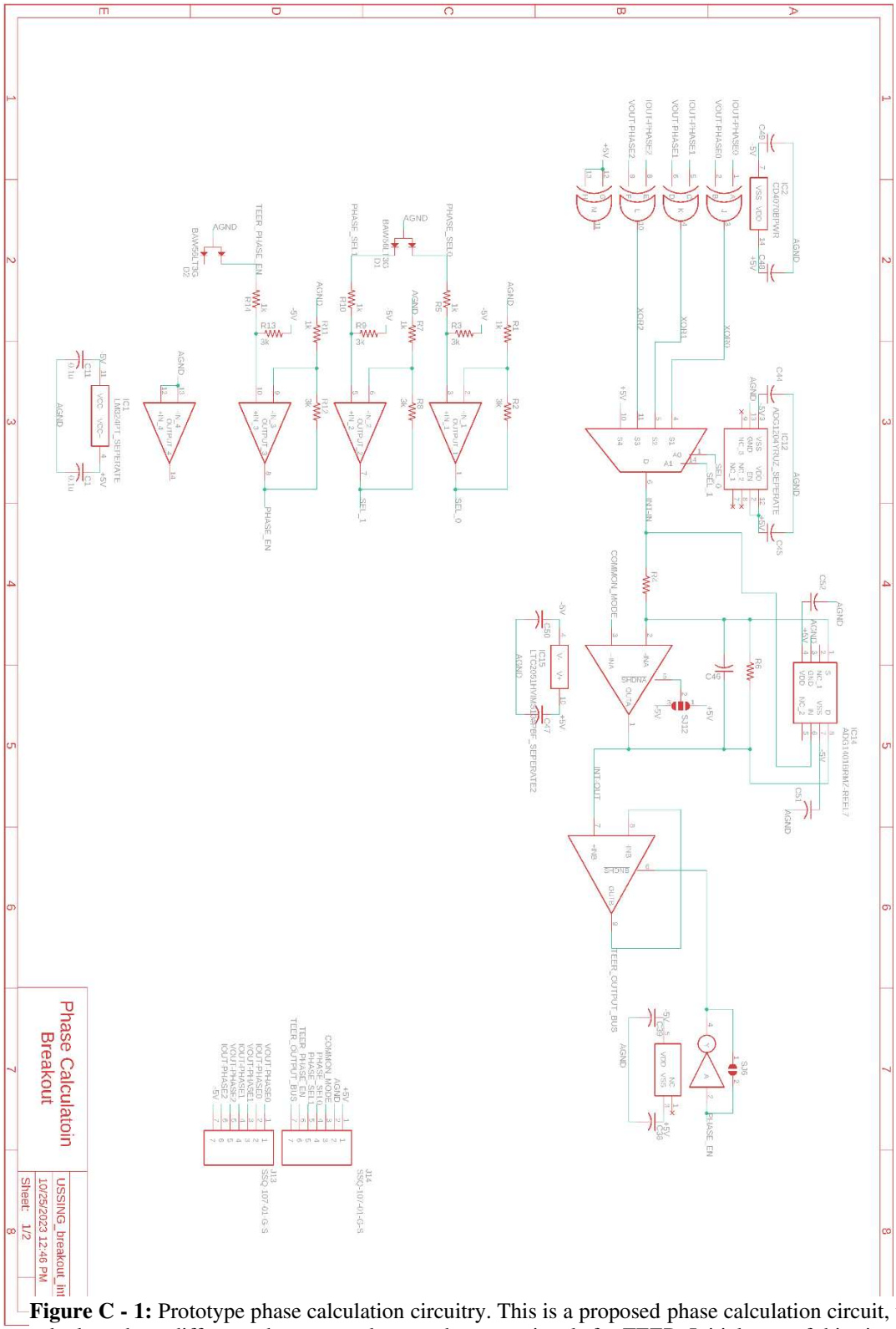

Figure C - 1: Prototype phase calculation circuitry. This is a proposed phase calculation circuit, to calculate phase difference between voltage and current signals for TEER. Initial tests of this circuit proved to be positive, but it was not used in the final design.

Appendix D – PCB Layouts

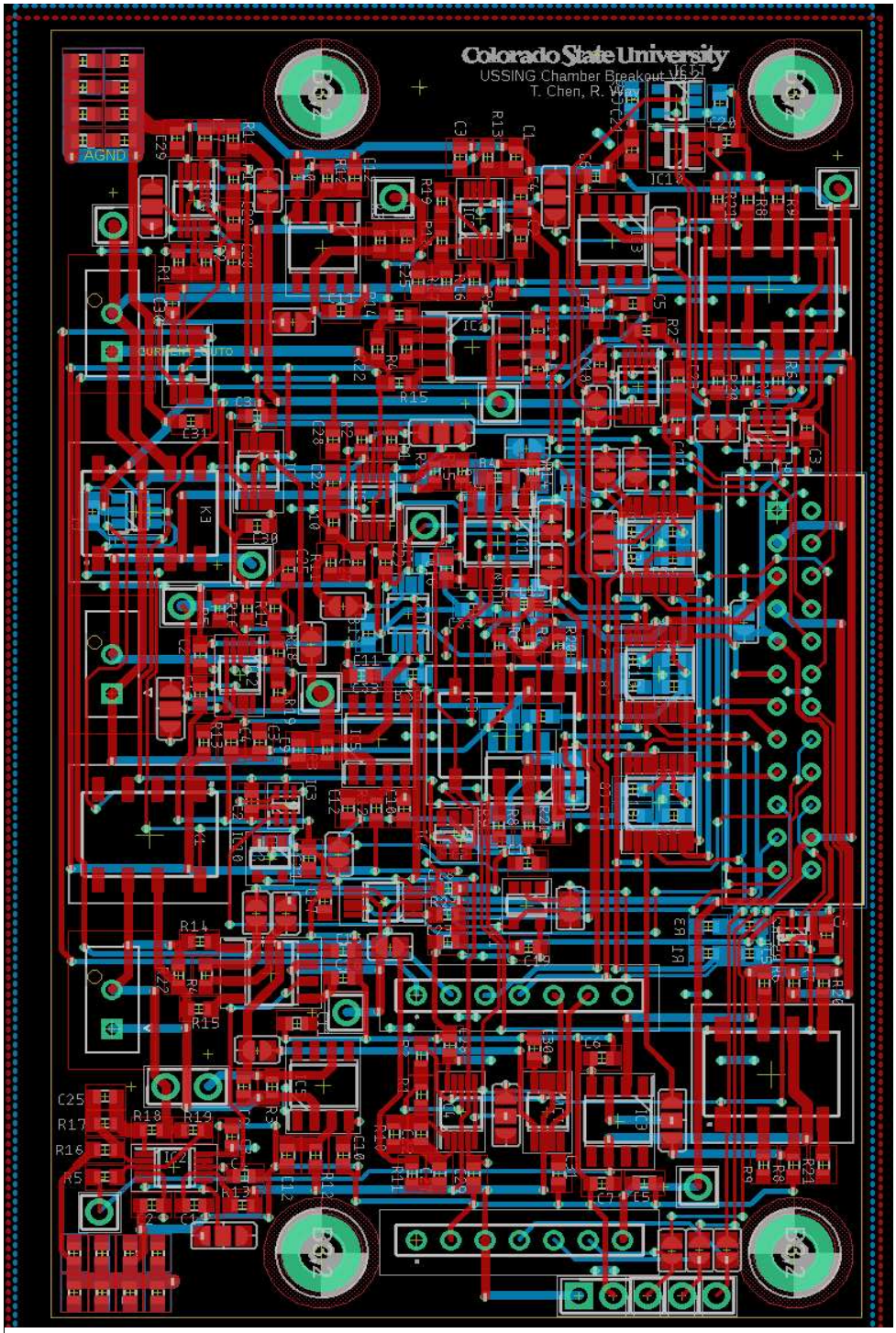

Figure D - 1: TEER calculation board layout

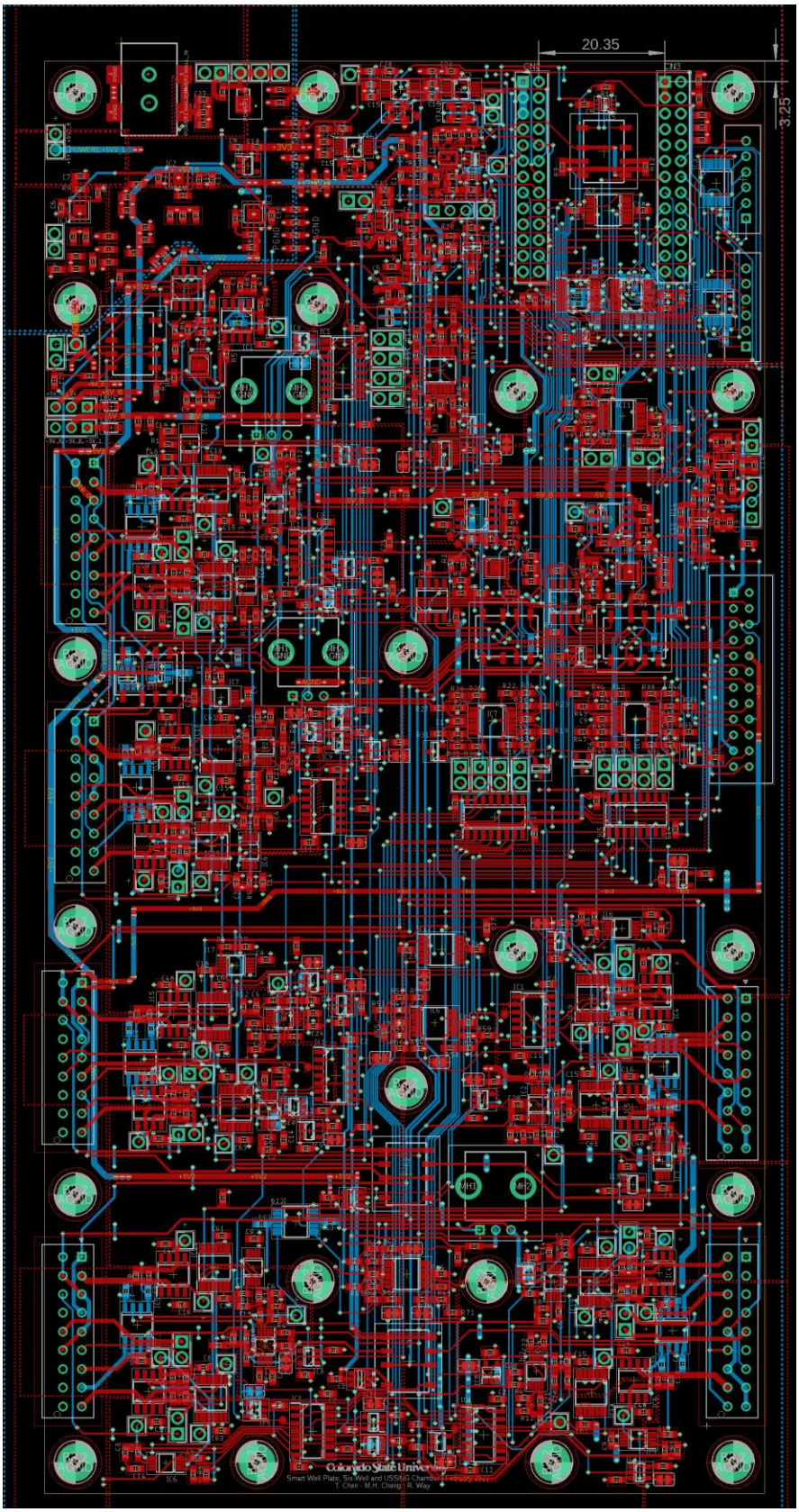

Figure D - 2: Main control board layout

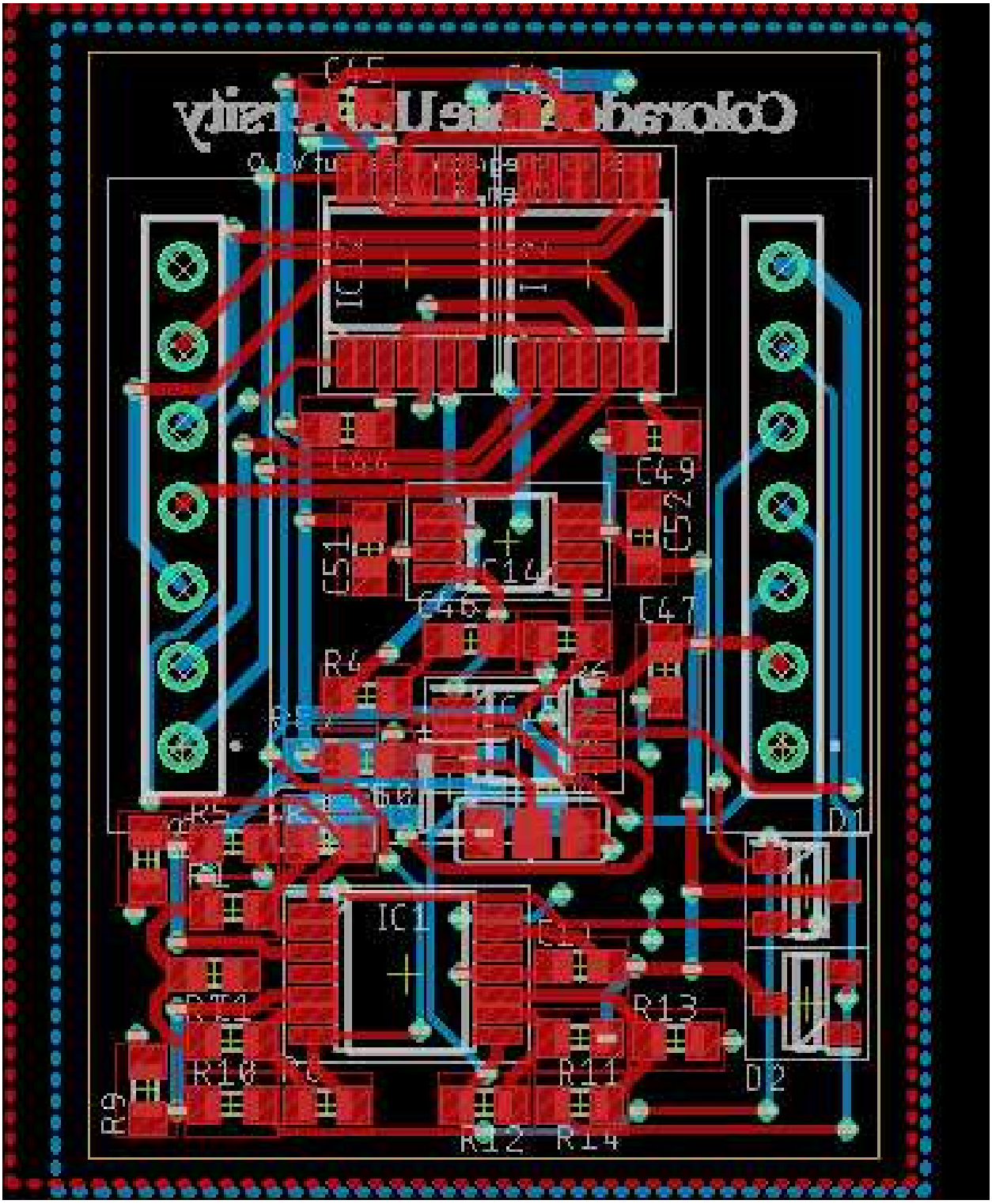

Figure D - 3: Phase calculation circuit layout